J. Fluid Mech. (1997), *vol.* 342, *pp.* 263–293. Printed in the United Kingdom

Small-scale characteristics of a turbulent boundary layer over a rough wall

By H. S. SHAFI AND R. A. ANTONIA
Department of Mechanical Engineering University of Newcastle, N.S.W., 2308, Australia

(Received 24 September 1996 and in revised form 10 February 1997)

Measurements of the spanwise and wall-normal components of vorticity and their constituent velocity derivative fluctuations have been made in a turbulent boundary layer over a mesh-screen rough wall using a four-hot-wire vorticity probe. The measured spectra and variances of vorticity and velocity derivatives have been corrected for the effect of spatial resolution. The high-wavenumber behaviour of the spectra conforms closely with isotropy. Over most of the outer layer, the normalized magnitudes of the velocity derivative variances differ significantly from those over a smooth wall layer. The differences are such that the variances are much more nearly isotropic over the rough wall than on the smooth wall. This behaviour is consistent with earlier observations that the large-scale structure in this rough wall layer is more isotropic than that in a smooth wall layer. Isotropy-based approximations for the mean energy dissipation rate and mean enstrophy are consequently more reliable in this rough wall layer than in a smooth wall layer. In the outer layer, the vorticity variances are slightly larger than those over a smooth wall; reflecting structural differences between the two flows.

1. Introduction

Experimental investigations of a turbulent boundary layer over a mesh-screen rough wall (Krogstad, Antonia & Browne 1992; Krogstad & Antonia 1994; Shafi & Antonia 1995; Shafi Antonia & Krogstad 1995) have indicated that the turbulence structure differs, in a number of ways, from that in a smooth wall boundary layer. For example, the magnitudes of $\overline{u_2^{+2}}$, the normal Reynolds stress, and of the Reynolds shear stress $\overline{u_1^+ u_2^+}$ (u_1, u_2 and u_3 are the velocity fluctuations in the streamwise x_1, wall-normal x_2 and spanwise x_3 directions respectively; the superscript + denotes normalization by the friction velocity U_τ) are larger than in a smooth wall layer. Two-point velocity correlations indicated that the average inclination of the large-scale motion is twice as large as on a smooth wall while the longitudinal length scale associated with this motion is considerably smaller over the rough wall. The relative magnitudes of the length scales in the x_1, x_2, and x_3 directions implied that the large-scale motion was closer to isotropy in the rough wall layer. The measured second and third invariants of the Reynolds stresses suggested that the anisotropy of the Reynolds stress tensor is appreciably reduced over the roughness (Shafi & Antonia 1995). Following these observations, one would expect the small-scale turbulence structure to be closer to isotropy in this rough wall layer. The major aim of this paper is to quantify this expectation by examining the measured statistics of velocity derivatives and vorticity fluctuations and comparing them to the corresponding isotropic values. As a defining

characteristic of turbulence, vorticity fluctuations ω_i ($\equiv \epsilon_{ijk}u_{k,j}$, where ϵ_{ijk} is the alternating unit tensor and $u_{k,j} \equiv \partial u_k/\partial x_j$ is the velocity gradient tensor) have been used for detecting the turbulent/non-turbulent interface (e.g. Corrsin & Kistler 1955; Klewicki, Falco & Foss 1992). Vorticity is also an important characteristic of the small-scale structure since the length scales which contribute most to the vorticity spectrum reside in the dissipative range (e.g. Antonia, Zhu & Shafi 1996*b*). Vorticity statistics should therefore be useful for checking departures from isotropy of the small-scale structure. Relatively few vorticity measurements have been reported for boundary layers over rough walls. Corrsin & Kistler (1955) used a Kovasznay-type vorticity probe to measure ω_1 over a corrugated wall; they reported the variations of $\overline{\omega_1^2}^{1/2}$ across the layer but the focus of their investigation was the turbulent/non-turbulent interface and its properties. Ong & Wallace (1995) presented spectra of all three components of ω_i in a rough wall boundary layer at a high turbulence Reynolds number R_λ ($\equiv \overline{u_1^2}\lambda/\nu$; λ is the Taylor microscale $\overline{u_1^2}^{1/2}/\overline{u_{1,1}^2}^{1/2}$ and ν is the kinematic viscosity) of 870, mainly with a view to compare the inertial-range behaviour with isotropy. Fan (1991) measured ω_1, using the Kovasznay-type probe, in the atmospheric surface layer, primarily to explore the multifractal nature of vorticity. Fan also reported that, over the inertial range, the spectrum of ω_1 was in agreement with isotropy. Folz (1993) reported measurements of $\overline{\omega_3^2}^{1/2}$ obtained with a four-hot-wire probe (Foss 1979) in a turbulent boundary layer over two rough surfaces, one comprising closely packed sifted rocks and the other a succession of spanwise square rods with a spacing to width ratio of 4. The distributions of $\overline{\omega_3^2}^{1/2}$, like those for the r.m.s. velocities, indicated differences in both inner and outer regions between the two surfaces. Krogstad & Antonia (1994) reported approximations to $\overline{\omega_2^2}^{1/2}$ and $\overline{\omega_3^2}^{1/2}$ over a mesh-screen roughness. These vorticity components were inferred from data obtained using orthogonal arrays of X-probes, one in the (x_1, x_2)-plane and the other in the (x_1, x_3)-plane. The spatial resolution of the array was poor ($\Delta x_2^* \simeq 66$ at $x_2/\delta \simeq 0.3$, δ is the boundary layer thickness; an asterisk denotes normalization by the Kolmogorov length scale $\eta \equiv \nu^{3/4}/\overline{\epsilon}^{1/4}$ and velocity scale $U_K = \nu^{1/4}\overline{\epsilon}^{1/4}$, where $\overline{\epsilon}$ is the mean energy dissipation rate), so the values of $\overline{\omega_2^2}^{1/2}$ and $\overline{\omega_3^2}^{1/2}$ were significantly underestimated. In all the previous studies, the data were not corrected for the effect of spatial resolution of the probe. It is important that adequately resolved data are available for comparison with the adequately resolved (experimental and direct numerical simulation (DNS)) data for a smooth wall layer.

An attempt is made to provide as reliable a set of vorticity data as possible by correcting some of the statistics (spectra, variances) for the effect of spatial resolution of the probe. It is expected that the observed differences in the large-scale motion between rough and smooth wall layers (Krogstad *et al.* 1992; Krogstad & Antonia 1994) should be reflected in the vorticity statistics. In particular, since the large-scale structure is more isotropic (Shafi & Antonia 1995) over the rough wall, the small-scale structure should also conform more closely with isotropy. An effective way of quantifying the departure from isotropy is to determine the invariants of the vorticity and velocity derivative tensors (e.g. Antonia & Kim 1994). Experimentally, this represents a formidable task. However, two components of ω_i and five components of $u_{i,j}$ were measured; the corrected spectra and variances of these quantities could be compared with the corresponding isotropic expressions and values. A second aim of this paper, not unrelated to the first, is to establish whether the nature of the surface can affect the small-scale structure in the outer layer. This is important in

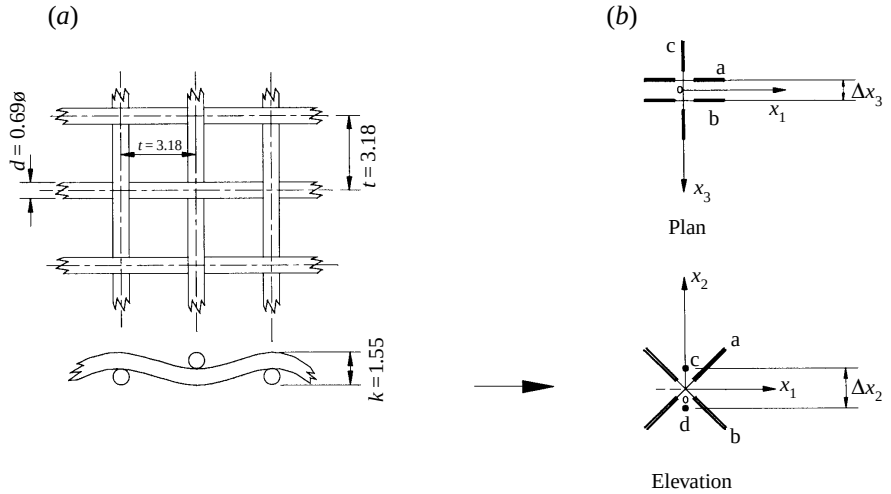

FIGURE 1. (*a*) Geometry of the mesh roughness, dimensions are in mm; (*b*) geometry of the four-hot-wire probe used for measuring ω_i ($i = 2$ and 3); a and b denote the X-wires while c and d denote the single hot wires. The geometry in the sketch corresponds to that used for ω_3 measurements.

the context of determining the degree of interaction between inner and outer regions of the layer. On the basis of Reynolds stresses and two-point correlations, the level of interaction over a mesh-screen rough wall appears to be much greater than on a smooth wall (Krogstad & Antonia 1994). This interaction should leave its signature on the small-scale structure.

Section 2 describes the experimental conditions and instrumentation. The effect of spatial resolution on the measurements of transverse derivatives of the longitudinal velocity fluctuations is considered in §3. Several checks carried out to ascertain the reliability of the present data are described in §4. Comparison with local isotropy is discussed in §5. Results for the variances of the transverse vorticity components and their associated velocity derivatives are presented in §6. P.d.f.s and higher-order moments of these quantities are reported in §7 while various approximations to the mean energy dissipation rate and mean enstrophy are examined in §8.

2. Experimental details

The measurements were made in a self-preserving turbulent boundary layer over a mesh roughened wall. The roughness consisted of a 3.53 m long woven stainless steel screen of thickness $k = 1.55$ mm with a wire spacing/diameter ratio of 4.61 (figure 1*a*). The boundary layer was tripped with a combination of a 4 mm diameter cylinder and a 150 mm wide strip of 40 grit abrasive paper. A detailed description of the experimental set-up and flow conditions is given in Krogstad *et al.* (1992). The data were obtained at a distance of 3.23 m from the end of the tunnel contraction. The pressure gradient was zero and the free-stream velocity U_∞ was nominally 10 m s^{-1}. The value of the friction velocity U_τ, inferred from the mean velocity profile using the optimization scheme of Krogstad *et al.*, was 0.52 m s^{-1}. Under these conditions, the value of the Reynolds number based on the momentum thickness θ and the Kármán number were respectively Re_θ ($\equiv U_\infty\theta/\nu$) $\simeq$ 7987 and δ^+ ($\equiv \delta U_\tau/\nu$) $\simeq$ 3152. The roughness Reynolds number k^+ ($\equiv kU_\tau/\nu$) is about 54. While this is comparable to

the value ($\simeq 55$) characterizing the upper transition limit for sand grain roughness, it has been shown (Hama 1954; Bandyopadhyay 1987) that a much lower limit ($\simeq 20$) applies to wire mesh roughness; the present flow can therefore be considered to be fully rough. The Kolmogorov scale η increased from 0.1 mm at $x_2/\delta \simeq 0.05$ to 0.17 mm at $x_2/\delta \simeq 0.66$; here $\bar{\epsilon}$ was approximated using isotropy, namely $\bar{\epsilon} = 15\nu\overline{u_{1,1}^2}$ (the results in §8 support this approximation). Over the same range of x_2/δ, the turbulence Reynolds number R_λ varied from about 175 to 210 and was approximately constant ($\simeq 250$) in the region $0.16 \leqslant x_2/\delta \leqslant 0.55$.

The spanwise and wall-normal vorticity components were obtained using a four-hot-wire vorticity probe consisting of an X-wire and two parallel single wires (e.g. Haw, Foss & Foss 1989; Rajagopalan & Antonia 1993). The two parallel wires were normal to the plane of the X-wire and straddled the intersection of the X-wire (figure 1*b*). For ω_3 measurements, the two single wires were placed in the x_3 direction, with a separation in the x_2 direction; the X-wire was in the (x_1, x_2)-plane (the probe was rotated by 90° for ω_2 measurements). The separation Δx_3 between the X-wires was about 0.95 mm ($\Delta x_3^* \simeq 7.7$ at $x_2/\delta \simeq 0.22$) and between the parallel wires Δx_2 was about 0.9 mm ($\Delta x_2^* \simeq 7.3$ at $x_2/\delta \simeq 0.22$). This latter value was chosen after assessing the effect of Δx_2^* on $\overline{u_{1,2}^2}$ (see §3). This choice was sufficiently large to avoid problems associated with small separations (e.g. noise contamination, possible flow interference) and allowed $\overline{u_{1,2}^2}$ to be corrected for the effect of spatial resolution. The included angle between the X-wires was about 110°, which was large enough to minimize the effect of large velocity cone angles (e.g. Perry, Lim & Henbest 1987; Browne, Antonia & Chua 1989) near the wall. All four (Wollaston Pt–10% Rh) wires of the probe had a diameter d of 2.5 μm. The wires were partially etched to a nominal length ℓ of 0.5 mm. The ratio $\ell/d = 200$ was sufficient for end conduction effects (Champagne, Sleicher & Wehrmann 1967) and the possible low-wavenumber attenuation (Paranthoen, Petit & Lecordier 1982) to be neglected.

The hot wires were operated with in-house constant-temperature anemometers at an overheat ratio of 1.5. The signals from the wires were filtered at a cut-off frequency f_c to minimize the contamination from high-frequency electronic noise. The value of f_c was identified, after examining the spectra of the differentiated signals on a real-time spectrum analyser (HP3582A), with the frequency at which the spectra were about 2–3 dB higher than the frequency where the noise starts to make a significant contribution. At $x_2/\delta \simeq 0.33$, f_c was about $0.9f_K$. The details of this procedure and the adequacy of the choice of f_c have been discussed in detail in Antonia *et al.* (1996*b*). The signals were amplified and then digitized at a sampling frequency of $2f_c$ into a personal computer using a 12 bit A/D converter. A record duration t_s of 60 s was used. Subsequent data processing was done on a VAX 8550 computer.

3. Selection of Δx_2 and the effect of spatial resolution

The measurement of vorticity is difficult primarily because of spatial resolution requirements. For the particular probe geometry considered in this investigation, the main difficulty relates to the selection of an appropriate value of the separation between the two parallel wires. Previous studies (e.g. Antonia, Zhu & Kim 1993; Zhu, Antonia & Kim 1993) have identified the problems involved in accurately measuring $\overline{u_{1,2}^2}$ (or $\overline{u_{1,3}^2}$) using a pair of parallel hot wires. A large separation attenuates the contribution from the small-scale motion to the high-wavenumber part of the $u_{1,2}$ spectrum and results in $\overline{u_{1,2}^2}$ and consequently $\overline{\omega_3^2}$ being underestimated. Wyngaard

(1969) suggested that in order to obtain accurate estimates of $\overline{u_{1,2}^2}$ with a two-parallel-wire probe, the value of Δx_2^* should be less than 3. Klewicki & Falco (1990) prescribed that Δx_2^* should be in the range $1.0 < \Delta x_2^* \leqslant 3.33$. George & Hussein (1991) suggested that the spatial dimensions of the probes used for velocity derivative measurements must be of order η.

While the above suggestions may be correct in theory, in practice too small a separation significantly overestimates $\overline{u_{1,2}^2}$ due to a number of errors. For very small separations (e.g. $\Delta x_2^* \leqslant 2$), the contamination from the electronic noise of the measuring equipment becomes significant, the uncertainties both in the measurement of the separation and the velocities increase and there is the possibility of flow interference from one probe to the other (e.g. Mestayer & Chambaud 1979; Browne, Antonia & Chambers 1983). Accordingly, it is necessary to select an optimum separation such that the effects of different errors are minimized. However, the value of this separation is dependent on the location of the probe in a particular flow and may also vary from one flow to another (Antonia & Mi 1993; Ewing, Hussein & George 1995). Therefore, it is important that the choice of an appropriate separation is made only after carefully assessing the effect of varying Δx_2^* (or Δx_3^*) on estimates of $\overline{u_{1,2}^2}$ (or $\overline{u_{1,3}^2}$).

When the separation Δx_2^* is such that the major source of error is the high-wavenumber attenuation of the spectrum, Wyngaard's analysis, see e.g. Wyngaard (1969), which assumes isotropy, provides a potential method for correcting measurements of $\overline{u_{1,2}^2}$. An extended version of the spectral correction scheme has been tested experimentally at the centreline of a fully developed turbulent channel flow and successfully 'calibrated' using the DNS data for the same flow (e.g. Zhu *et al.* 1993). This technique has also been employed in a turbulent wake flow (Mi & Antonia 1996) and a round jet (Antonia & Mi 1993). The results provide satisfactory support for the technique, at least when isotropy is reasonably approximated by the high-wavenumber end of the spectrum.

In view of the preceding comments, it seems appropriate to assess the effect of separation on the measurements of $u_{1,2}$ for the present four-hot-wire vorticity probe. Accordingly, a series of separate experiments was carried out at several wall-normal locations in the rough wall layer, to decide on the appropriate Δx_2 separation for the vorticity probe. For this purpose, two parallel wires, aligned in the x_3 direction and separated in the x_2 direction were used to measure $u_{1,2}$ using the finite difference approximation ($\equiv \Delta u_1/\Delta x_2$). Both wires could be moved an equal distance, using two independent traversing mechanisms with least counts of 0.01 mm, so that the midpoint between the wires remained at the same location.

Measurements were made at four locations ($x_2/\delta \simeq 0.05$, 0.11, 0.22, 0.33) in the rough wall layer, for a relatively large range of Δx_2^* values. The separation Δx_2 was varied in the range 0.3–2.2 mm which corresponded to $3 \leqslant \Delta x_2^* \leqslant 22$ at $x_2/\delta \simeq 0.05$. The effect of wire separation Δx_2^* on $\phi_{u_{1,2}}^m$, the measured spectrum of $u_{1,2}$ can be observed in figures 2(*a*) and 2(*b*). Only results for $x_2/\delta \simeq 0.05$ and 0.33 are shown in the figures. The normalization is such that $\int \phi_{u_{1,2}}^* \mathrm{d}k_1^* = \overline{u_{1,2}^{*\,2}}$. As expected, $\phi_{u_{1,2}}^m$ shows an increased attenuation at high wavenumbers as Δx_2^* increases. For each x_2/δ location, the corrected spectra are also shown in the figures. The details of the correction procedure can be found in Antonia & Mi (1993) and are not repeated here. The correction scheme assumes that $E(k)$, the three-dimensional energy spectrum tensor, is known. Here, $E(k)$ was determined using the measured distribution of ϕ_{u_1},

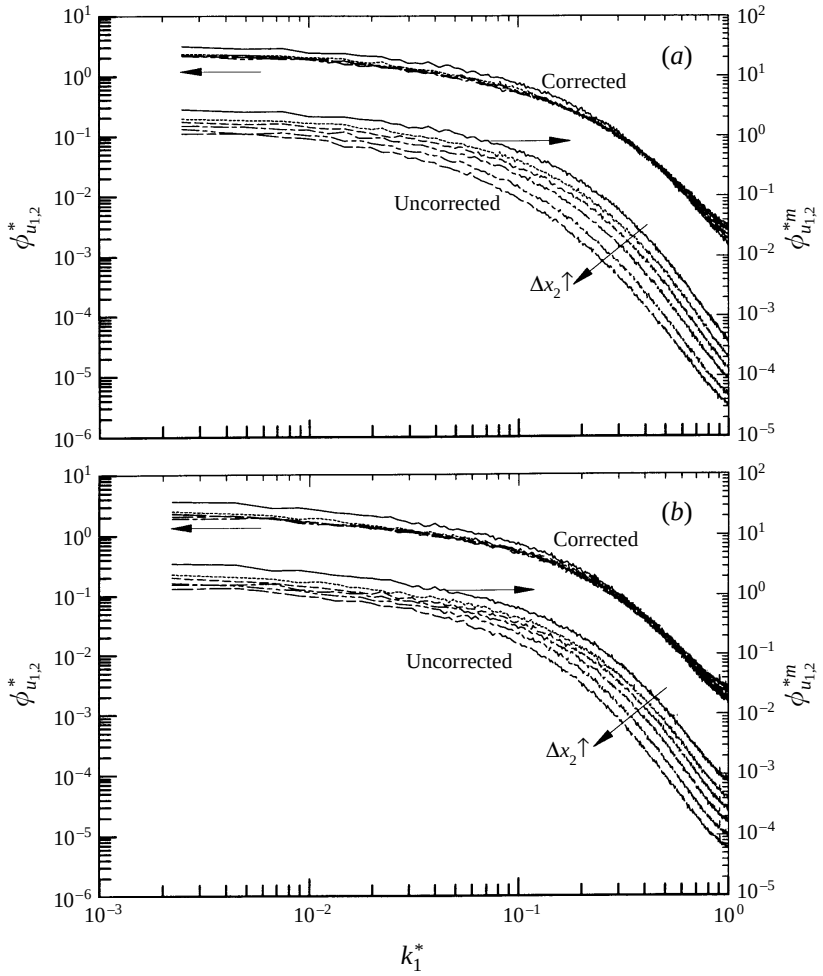

FIGURE 2. Measured spectra of $u_{1,2}$. Both uncorrected and corrected spectra are shown. (*a*) $x_2/\delta \simeq 0.05$: —, $\Delta x_2^* = 5$; - - -, 7; – –, 9; — - —, 12; — - - —, 17; — – —, 22. (*b*) $x_2/\delta \simeq 0.33$: —, $\Delta x_2^* = 3.8$; - - -, 5.3; – –, 6.8; — - —, 9.0; — - - —, 12.0; — – —, 16.6.

the spectrum of u_1, via the isotropic relation

$$E(k) = k^2 \left(\frac{\partial^2 \phi_{u_1}}{\partial k_1^2} \right)_{k_1=k} - k \left(\frac{\partial \phi_{u_1}}{\partial k_1} \right)_{k_1=k} \quad , \tag{3.1}$$

where $k \equiv (k_1^2 + k_2^2 + k_3^2)^{1/2}$ is the modulus of the wavenumber vector $\boldsymbol{k}$. Apart from the data for the smallest separations, at each x_2/δ location all corrected $\phi_{u_{1,2}}$ data for different Δx_2^* values are in reasonably good agreement with each other. The collapse of different corrected $\phi_{u_{1,2}}$ implies the existence of a unique value for $\overline{u_{1,2}^2}$. It also corroborates the correction technique. The data for $\Delta x_2^* = 5$ (figure 2*a*) and 3.8 (figure 2*b*) suffer from the problems associated with too small a separation. The application of corrections to these data, therefore, would result in an overestimation of the spectral densities.

The dependence of the measured values of $\overline{u_{1,2}^2}^{-1/2} \delta / U_\tau$ on Δx_2^* at $x_2/\delta \simeq 0.05$ and 0.33 is shown in figure 3. Also plotted are the corrected values of the data for

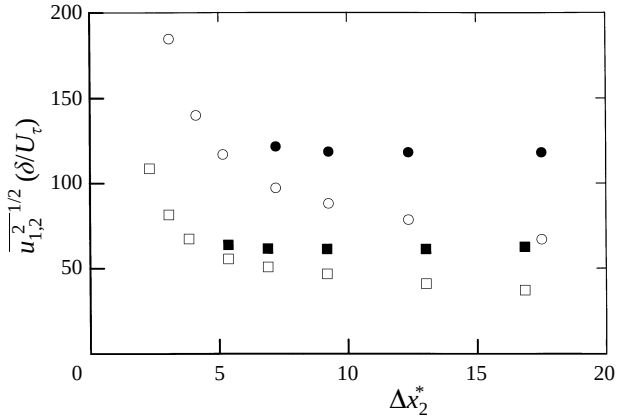

FIGURE 3. Dependence of $\overline{u_{1,2}^2}^{1/2}\delta/U_\tau$ on Δx_2^*. ○, $x_2/\delta \simeq 0.05$; □, 0.33. Open and filled in symbols are for uncorrected and corrected data respectively.

separations greater than about 7η ($x_2/\delta \simeq 0.05$) and 5η ($x_2/\delta \simeq 0.33$). For each x_2/δ, the corrected values are within 5% of each other implying a plateau for $\overline{u_{1,2}^2}$. This is consistent with the spectral data in figures 2(*a*) and (*b*). The results indicate that for the present experimental conditions, a separation of $7\eta \sim 9\eta$ for the two parallel wires would allow reliable estimates of $\overline{u_{1,2}^2}$ to be obtained, provided a correction is applied for the effect of separation. These values of Δx_2^* are significantly different from those suggested by Klewicki & Falco ($1 < \Delta x_2^* \leqslant 3.33$), George & Hussein ($\Delta x_2^* \sim 1$) and Antonia *et al.* (1993) ($2 \leqslant \Delta x_2^* \leqslant 3$). Clearly, the use of any of the previous recommendations for selecting Δx_2^* would have resulted in $\overline{u_{1,2}^2}$ being overestimated in the present flow. This underlines the need to carry out a separate experiment in order to choose the most appropriate value of Δx_2^* for a particular flow, in accordance with the suggestion of Ewing *et al.* (1995). Such an investigation, therefore, seems to be a necessary first step for measuring vorticity using a four-hot-wire probe.

Antonia *et al.* (1996*b*) extended the correction procedure for $u_{1,2}$ to the measurement of the lateral components of ω_i. The method takes into account all the geometrical parameters of the probe, including the effects of Δx_2^*, Δx_3^* and ℓ^*. The attenuation of the measured vorticity spectrum increases as the wavenumber increases but does not vanish when the wavenumber is zero. The correction procedure has been successfully tested using the measurement of ω_i ($i = 2$ and 3) near the end of the intermediate region of a wake. Although the correction invokes local isotropy, the major contributor to the high-wavenumber part of the ω_i ($i = 2$ and 3) spectrum is the streamwise derivative of the lateral velocity fluctuation. Since the correction of $\phi_{u_{2,2}}$ or $\phi_{u_{3,1}}$ does not involve the assumption of local isotropy, the correction of the ω_i spectrum should be unaffected by this assumption. The details of the correction procedure are outlined in Antonia *et al.* (1996*b*).

4. Accuracy checks

A number of checks were carried out in order to ascertain the reliability of the present data. The distributions of $\overline{u_1^{+2}}^{1/2}$ obtained from the X-wires and the two parallel wires were in good agreement with those obtained with a single wire. The

measured distributions of $\overline{u_2^{+2}}^{1/2}$ and $\overline{u_3^{+2}}^{1/2}$ were within 15% and 10% respectively of those reported in Krogstad *et al.* (1992). The experimental uncertainties in estimates of $\overline{u_1^{+2}}^{1/2}$, $\overline{u_2^{+2}}^{1/2}$ and $\overline{u_3^{+2}}^{1/2}$ are 7%, 16% and 12% respectively. These estimates were obtained from the scatter in 15 data sets obtained in different runs with different single hot wires, X-wires and V-probes. For high wavenumbers, the u_2 and u_3 spectra showed good agreement with the DNS channel flow data (Kim & Antonia 1993). In addition, the measured $\phi^*_{u_{1,2}}$ obtained from the two wires of the vorticity probe were in good agreement with those calculated from the separate two-parallel-wire experiment (§3).

Digital records of ω_2 and ω_3 were obtained from the measurements of u_i using the approximations

$$\omega_2 \equiv u_{1,3} - u_{3,1} \simeq \frac{\Delta u_1}{\Delta x_3} + \frac{1}{\overline{U}_1}\frac{\Delta u_3}{\Delta t} \tag{4.1}$$

and

$$\omega_3 \equiv u_{2,1} - u_{1,2} \simeq -\frac{1}{\overline{U}_1}\frac{\Delta u_2}{\Delta t} - \frac{\Delta u_1}{\Delta x_2}\,. \tag{4.2}$$

Here, Δt ($\equiv f_s^{-1}$) is the sampling time interval. Forward difference temporal differentiation was used with the magnitude of $\overline{U}_1\Delta t$ roughly half that of Δx_2 (or Δx_3); at $x_2/\delta = 0.22$, $\overline{U}_1\Delta t = 0.41$ mm whereas $\Delta x_2 = 0.9$ mm. Central difference differentiation with $\overline{U}_1\Delta t \simeq \Delta x_2$ (or Δx_3) would have advantages in terms of minimizing phase distortions (e.g. Wallace & Foss 1995); this could be important when calculating velocity–vorticity correlations for example. We checked however that the statistics of ω_2 (and ω_3) were the same with both types of differentiation. Taylor's hypothesis

$$u_{i,1} \equiv -\frac{1}{\overline{U}_1}u_{i,t} \tag{4.3}$$

was used to convert time derivatives into x_1-derivatives. Piomelli, Balint & Wallace (1989) have investigated the validity of this hypothesis using the databases generated by DNS and large-eddy simulations (LES) of turbulent channel flow as well as measurements in a boundary layer. They concluded that the hypothesis is valid for $x_2^+ \geqslant 15$ (+ denotes normalization by U_τ and ν). Kim & Hussain's (1992) results are also consistent with this conclusion. Recently, additional support for the applicability of the hypothesis in the region $x_2^+ \geqslant 15$ was provided by two-point LDA velocity correlations (Elavarasan, Djenidi & Antonia 1996). Although a direct check of Taylor's hypothesis was not made in the present experiments, the previous results suggest that the hypothesis should be a good approximation, at least in the outer region.

No correction was applied to the X-wire data for the possible effect of $\overline{U}_{1,2}$. The magnitude of the ratio between the maximum value of $|u_{1,2}|$ and $\overline{U}_{1,2}$ at $x_2/\delta \simeq 0.03$, the location closest to the wall for the present measurements, is about 20. Consequently, the two parallel wires should adequately resolve the fluctuating velocity gradient though not the mean velocity gradient (Antonia, Browne & Shah 1988). The effect of the cross-stream velocity on the X-wire was also neglected. Vukoslavcevic & Wallace (1981) have indicated that for $x_2^+ \leqslant 50$, the influence of the instantaneous velocity gradients and cross-stream velocity may cause large errors in the streamwise vorticity component measured with a modified Kovasznay-type probe. Moin & Spalart (1987) used a numerical database to study the response of an X-probe in a boundary layer and found that errors caused by neglecting u_3 were important. On the other hand, Suzuki & Kasagi (1990), using their DNS database for a channel flow ($h^+ = 150$,

h is the channel half-width), concluded that the effect of u_3 was minimal. Foss, Ali & Haw (1987) have studied the effect of the transverse velocity component (U_3) on the measurement of ω_3 using a four-hot-wire probe. They concluded that this effect does not adversely affect the measurement of ω_3.

An estimate of the residual vorticity measured by the present probe can be inferred from the value of $\overline{\omega_2^2}^{1/2}$ (or $\overline{\omega_3^2}^{1/2}$) in the free stream (e.g. Haw *et al.* 1989; Klewicki *et al.* 1992). Since the present measurements were made only up to $x_2/\delta \simeq 1.0$, only rough (and conservative) estimates of the residual vorticity could be inferred. The ratios between the r.m.s. vorticity values at $x_2/\delta \simeq 1.0$ and those at $x_2/\delta \simeq 0.44$ were about 20 (for ω_3) and 17 (for ω_2) respectively. Klewicki *et al.* (1992) reported that the extrapolated value of $\overline{\omega_3^2}^{1/2}$ at $x_2/\delta \simeq 1.4$ was 9.7% of that measured at $x_2/\delta \simeq 0.58$. They pointed out that this estimate includes both the effects of the least-significant-bit (LSB), associated with the A/D converter, and the background noise.

Klewicki & Falco (1990) suggested that $t_s\overline{U}_1/\delta$ should be about 3500 in order to estimate the skewness and flatness factors of velocity derivatives and vorticity with an accuracy of $\pm 5\%$. The present value of $t_s\overline{U}_1/\delta$ is about 6600. Since $t_s\overline{U}_1/\delta$ is an integral time scale representative of large-scale motions, its use as a convergence criterion for small-scale statistics may not be entirely appropriate. Following Antonia, Satyaprakash & Hussain's (1982) recommendation, the time required for each moment to converge to within 5% of its final value was estimated. At $x_2/\delta \simeq 0.2$, about 30% of the total record duration was sufficient for convergence to within 5% of the final values of S_α and F_α ($\alpha = u_{1,1}$, $u_{1,2}$, $u_{2,1}$ and ω_3).

5. Checks of local isotropy

Antonia, Anselmet & Chambers (1986) pointed out that different tests may have different levels of sensitivity and therefore provide different indicators of the deviation from local isotropy. For example, second-order derivatives should provide a more stringent test than first-order derivatives since the former give more weighting to the high-wavenumber end of the spectrum.

Both the velocity and vorticity are solenoidal quantities (Batchelor 1953; Monin & Yaglom 1975; Antonia & Kim 1994) and consequently the corresponding isotropic relations have similar forms, namely

$$\phi_{u_2}(k_1) = \phi_{u_3}(k_1) = \frac{1}{2}\left(\phi_{u_1} - k_1\frac{\partial\phi_{u_1}}{\partial k_1}\right), \tag{5.1}$$

$$\phi_{\omega_2}(k_1) = \phi_{\omega_3}(k_1) = \frac{1}{2}\left(\phi_{\omega_1} - k_1\frac{\partial\phi_{\omega_1}}{\partial k_1}\right). \tag{5.2}$$

$\phi_{\omega_1}(k_1)$ can be expressed in terms of ϕ_{u_1} or $\phi_{u_{1,1}}$ (e.g. Van Atta 1991; Kim & Antonia 1993):

$$\phi_{\omega_1}(k_1) = \phi_{u_{1,1}}(k_1) + 4\int_{k_1}^{\infty}\frac{\phi_{u_{1,1}}(k)}{k}\mathrm{d}k, \tag{5.3}$$

$$\phi_{\omega_2}(k_1) = \phi_{\omega_3}(k_1) = \tfrac{5}{2}\phi_{u_{1,1}}(k_1) - \frac{k_1}{2}\frac{\partial\phi_{u_{1,1}}(k_1)}{\partial k_1} + 2\int_{k_1}^{\infty}\frac{\phi_{u_{1,1}}(k)}{k}\mathrm{d}k\,. \tag{5.4}$$

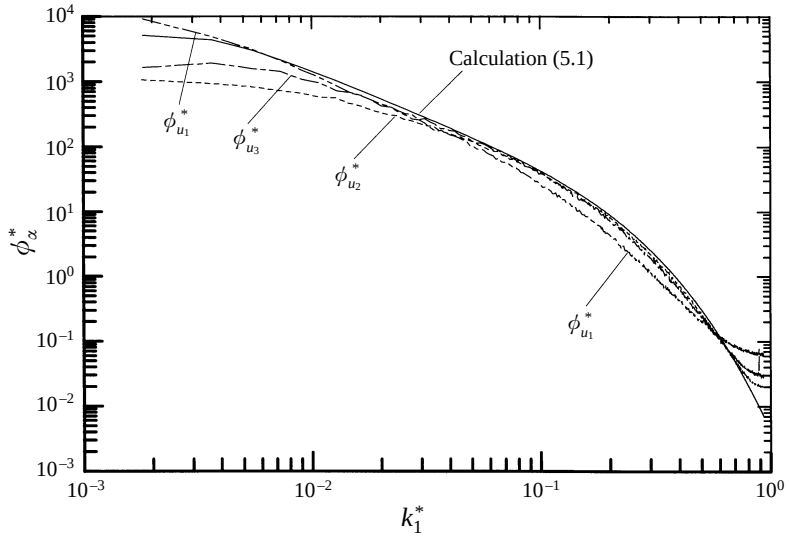

FIGURE 4. Comparison between measured u_2 and u_3 spectra and isotropic calculation at $x_2/\delta \simeq 0.44$. The spectra of u_1 are also shown.

The components of $\phi_{\omega_2}(k_1)$ and $\phi_{\omega_3}(k_1)$ may be written as follows:

$$\phi_{u_{1,2}}(k_1) = \phi_{u_{1,3}}(k_1) = 2\int_{k_1}^{\infty} \frac{1}{k}\phi_{u_{1,1}}(k)\mathrm{d}k, \tag{5.5}$$

$$\phi_{u_{2,1}}(k_1) = \phi_{u_{3,1}}(k_1) = \tfrac{3}{2}\phi_{u_{1,1}}(k_1) - \tfrac{1}{2}k_1\frac{\partial\phi_{u_{1,1}}}{\partial k_1}, \tag{5.6}$$

$$Co_{u_{1,2}u_{2,1}}(k_1) = Co_{u_{1,3}u_{3,1}}(k_1) = -\tfrac{1}{2}\phi_{u_{1,1}}(k_1)\,. \tag{5.7}$$

The measured spectra of u_2 and u_3, normalized such that $\int \phi^*_\alpha \mathrm{d}k_1^* = \overline{\alpha^{*2}}$ ($\alpha \equiv u_1$, u_2 or u_3), are plotted in figure 4 for $x_2/\delta \simeq 0.44$. For $k_1^* \geqslant 0.05$, $\phi^*_{u_2}$ and $\phi^*_{u_3}$ follow each other closely, in accord with isotropy (and with the less stringent condition of axisymmetry, as noted in Antonia *et al.* 1996*b*). In the same wavenumber range, there is reasonable agreement between the measured $\phi^*_{u_2}$ (or $\phi^*_{u_3}$) and the isotropic calculation using the measured $\phi^*_{u_1}$ (equation (5.1)). Least-square polynomial fits of $\phi^*_{u_1}$ of the form

$$\ln\phi^*_{u_1} = a_0 + a_1(\ln k_1^*) + \cdots a_n(\ln k_1^*)^n \tag{5.8}$$

were used for the calculations in (5.1). The maximum deviation between the measured and calculated $\phi^*_{u_2}$ is about 15%. The upturning of $\phi^*_{u_2}$ and $\phi^*_{u_3}$ for $k_1^* \geqslant 0.7$ is due to electronic noise. The discrepancy between $\phi^*_{u_2}$ and $\phi^*_{u_3}$ (as well as with the calculation) at low wavenumbers is expected since it reflects the influence of large-scale motions. For isotropy, $Co^*_{u_1u_2}$, the normalized u_1u_2 cospectrum should be zero, although the stringency of this test may be questionable (e.g. Mestayer 1982). At $x_2/\delta \simeq 0.44$, the magnitude of $Co^*_{u_1u_2}$ (figure 5) is nearly zero at $k_1^* \simeq 0.1$ although small negative values occur in the range $0.1 \leqslant k_1^* \leqslant 0.4$. This behaviour has also been observed in the $Co_{u_1u_2}$ data obtained in a low-Reynolds-number duct flow (Antonia *et al.* 1992) and a high-Reynolds-number rough-wall boundary layer (Antonia & Raupach 1993). Antonia *et al.* (1992) speculated that this behaviour probably reflects the presence

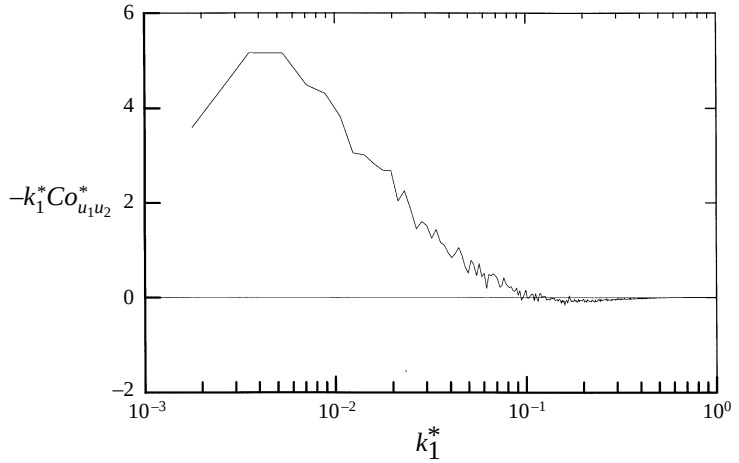

FIGURE 5. Measured u_1u_2 cospectrum at $x_2/\delta \simeq 0.44$.

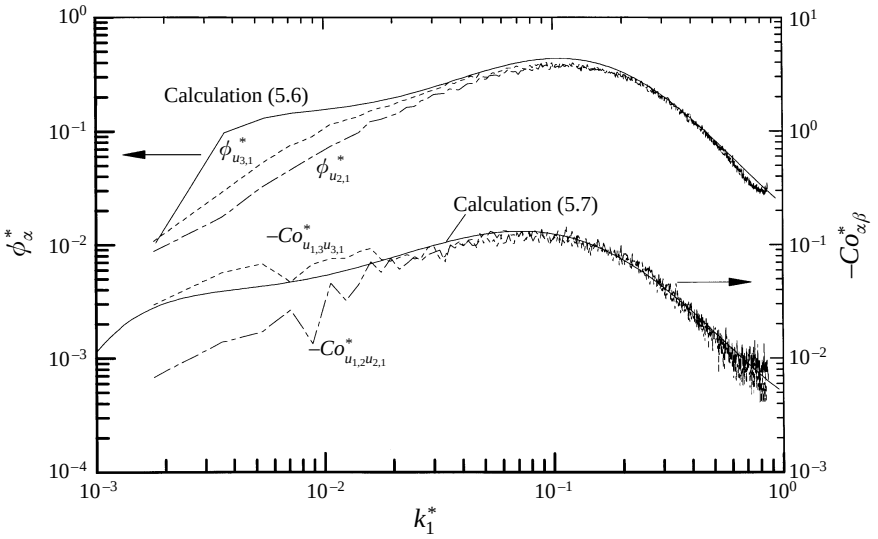

FIGURE 6. Comparison between the corrected distributions of $\phi_{u_{2,1}}$, $\phi_{u_{3,1}}$, $-Co_{u_{1,2}u_{2,1}}$ and $-Co_{u_{1,3}u_{3,1}}$ and the corresponding isotropic calculations at $x_2/\delta \simeq 0.44$.

of small-scale eddies which carry a small shear stress of opposite sign to that of the mean shear.

By comparison to the velocity spectra, velocity derivative and vorticity spectra, which receive larger contributions from the small-scale motions, should provide a more sensitive isotropy test (Antonia & Kim 1994). Figures 6 and 7 compare the corrected spectra of ω_i and their components with the corresponding isotropic calculations ((5.4)–(5.7)). The present corrected $\phi^*_{u_{1,1}}$ data were used for the calculation. The distributions of $\phi^*_{u_{2,1}}$ and $\phi^*_{u_{3,1}}$ (figure 6) are identical for $k_1^* \geqslant 0.1$. There is also good agreement between the present data and the isotropic calculation (5.6) in the high-wavenumber range. The corrections to the spectra of $u_{i,1}$ do not involve the assumption of local isotropy (Antonia *et al.* 1996*b*). The present results, therefore,

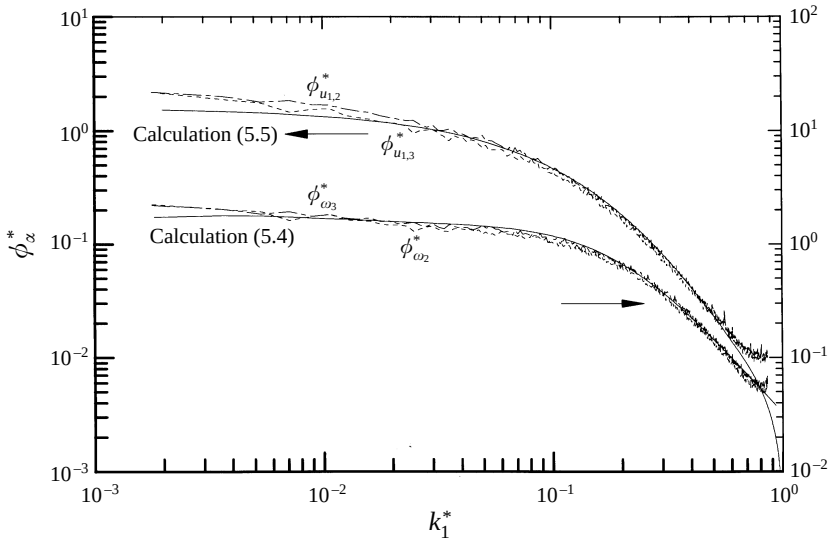

FIGURE 7. Comparison between corrected distributions of $\phi_{u_{1,2}}$, $\phi_{u_{1,3}}$, ϕ_{ω_3} and ϕ_{ω_2} and the corresponding isotropic calculations at $x_2/\delta \simeq 0.44$.

provide important support for local isotropy at sufficiently large k_1^*. For the present $Co^*_{u_{1,2}u_{2,1}}$ and $Co^*_{u_{1,3}u_{3,1}}$, the agreement between corrected distributions and calculation (5.7) begins at $k_1^* \simeq 0.05$. Since local isotropy is satisfied by the $u_{2,1}$ and $u_{3,1}$ spectra, one would expect that it should also hold for other velocity derivative spectra. Figure 7 shows that the corrected spectra of $u_{1,2}$ and $u_{1,3}$ follow each other quite closely for large wavenumbers; the agreement between the data and the calculation (5.5) applies for $k_1^* \geqslant 0.03$. The corrected distributions of ϕ_{ω_2} and ϕ_{ω_3} (figure 7) are almost identical, satisfying the isotropic condition $\phi_{\omega_2}(k_1) = \phi_{\omega_3}(k_1)$. This near equality between ϕ_{ω_2} and ϕ_{ω_3} also satisfies the less stringent requirement of axisymmetry. The isotropic calculation (5.4) is in good agreement with the data. The level of agreement with isotropy indicated in figures 6 and 7 has also been found at smaller x_2/δ (0.11, 0.22 and 0.33).

Antonia *et al.* (1996*b*) pointed out that the correction to the spectra of ω_3 (or ω_2) does not depend on the assumption of isotropy since the correction to $\phi_{u_{2,1}}$, the largest contributor to ϕ_{ω_3} at large k_1^*, does not involve the assumption of isotropy. Figure 8 shows the corrected spectra of ω_3 and its three components at $x_2/\delta \simeq 0.44$. The present distributions indeed confirm that $\phi^*_{u_{2,1}}$ is the major high-wavenumber contributor to $\phi^*_{\omega_3}$ while $\phi^*_{u_{1,2}}$ provides the major contributions at lower wavenumbers. This behaviour is also true for the uncorrected data. At $k_1^* \simeq 0.6$, $\phi^*_{u_{2,1}}$ represents 56% of $\phi^*_{\omega_3}$; $\phi^*_{u_{1,2}}$ and $-2Co^*_{u_{1,2}u_{2,1}}$ represent 26% and 18% of $\phi^*_{\omega_3}$ respectively. The conclusion of Antonia *et al.* (1996*b*), that the correction to ϕ_{ω_3} (or ϕ_{ω_2}) does not depend on local isotropy, should, therefore, apply to the present data.

Previous studies (e.g. Corrsin 1958; Antonia & Kim 1994) have suggested that the departure from isotropy may depend on the value of the suitably normalized mean shear S ($\equiv \overline{U}_{1,2}$). There are several possibilities for non-dimensionalizing S. For example, it is common to use the parameter $S\overline{q^2}/\overline{\epsilon}$ (where $\overline{q^2} = \overline{u_1^2} + \overline{u_2^2} + \overline{u_3^2}$) which represents the ratio between the time scale of the large-scale motion and that

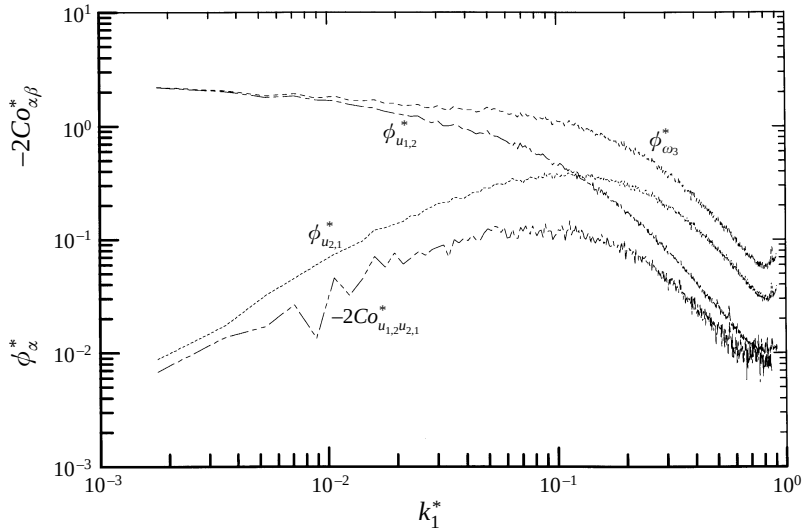

FIGURE 8. Corrected spectra of ω_3 and components at $x_2/\delta \simeq 0.44$.

of mean deformation (e.g. Moin 1990; Lee, Kim & Moin 1990). Durbin & Speziale (1991) have argued that the dissipation rate tensor cannot be isotropic if $S\overline{q^2}/\overline{\epsilon} \neq 0$. Kim & Antonia (1993) found that local isotropy was reasonably satisfied for velocity and pressure spectra at high wavenumbers with a value of $S\overline{q^2}/\overline{\epsilon}$ of about 6 (at $x_2/h \simeq 0.4$, where h is the channel half-width). For the spectral data presented in figures 4–7, whose behaviour in the high-wavenumber ends is consistent with local isotropy, the value of $S\overline{q^2}/\overline{\epsilon}$ ($\simeq 11.3$) is not negligible. One disadvantage of using $S\overline{q^2}/\overline{\epsilon}$, as pointed out by Antonia & Kim (1994), is that its value is zero at the wall, where S is maximum.

Uberoi (1957) suggested the use of $S/\overline{u_{1,2}^2}^{1/2}$, where $\overline{u_{1,2}^2}^{1/2}$ would reflect the anisotropy of the fluctuating velocity gradient. Corrsin (1958) non-dimensionalized S using the Kolmogorov time scale $(\overline{\epsilon}/\nu)^{-1/2}$. He argued that for local isotropy to be a good approximation, it is necessary that $S(\nu/\overline{\epsilon})^{1/2} \ll 1$. Using the DNS data, Antonia & Kim (1994) showed that in the near-wall region of a turbulent channel flow, $S(\nu/\overline{\epsilon})^{1/2}$ is better behaved than $S\overline{q^2}/\overline{\epsilon}$. Their results indicated that for vorticity to satisfy local isotropy, Corrsin's (1958) criterion can be relaxed to $S(\nu/\overline{\epsilon})^{1/2} \leqslant 0.2$. At $x_2/\delta \simeq 0.44$, $S(\nu/\overline{\epsilon})^{1/2}$ is about 0.1. This is consistent with the expectation that local isotropy is a good approximation for dissipative wavenumbers ($k_1^* \gtrsim 0.1$), provided $S(\nu/\overline{\epsilon})^{1/2}$ is small (Sreenivasan & Antonia 1997).

Saddoughi & Veeravalli (1994) reported that the wavenumber at which $Co_{u_1u_2}$ first satisfies local isotropy is $k_1(\overline{\epsilon}/S^3)^{1/2} \simeq 10$; this limit can be relaxed to $k_1(\overline{\epsilon}/S^3)^{1/2} \simeq 3$ for velocity spectra. Their measurements were taken in a high-Reynolds-number ($R_\lambda \simeq 1450$) rough-wall boundary layer at $x_2/\delta \simeq 0.4$. For the present data, the corresponding limit is about 15 for $Co_{u_1u_2}$. This larger value, compared with that of Saddoughi & Veeravalli, reflects the smaller value of R_λ ($\simeq 250$) in our flow. As R_λ increases, the extent of the inertial range increases and isotropy should be satisfied at smaller wavenumbers. For the present ϕ_{ω_i} ($i = 2, 3$) data, the lower limit for $k_1(\overline{\epsilon}/S^3)^{1/2}$ can be relaxed to 1.

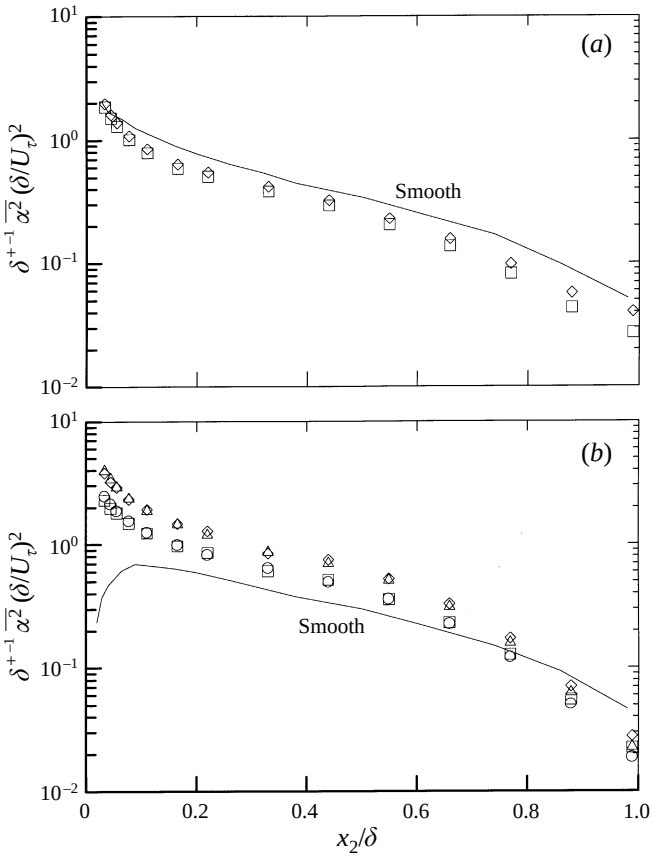

FIGURE 9. Comparison between normalized distributions of $\overline{u_{i,j}^2}$ over the smooth and rough walls. Rough wall, uncorrected data : □, ○; corrected data : ◇, △. Smooth wall, only uncorrected data are shown. (*a*) Rough wall : $\alpha = u_{1,1}$; $\delta^+ = 3552$. Smooth wall : —, $\alpha = u_{1,1}$, $\delta^+ = 555$. (*b*) Rough wall : □, ◇, $\alpha = u_{2,1}$; ○, △, $u_{3,1}$. Smooth wall : —, $\alpha = u_{2,1}$.

6. Results for $\overline{\omega_i^2}$ and $\overline{u_{i,j}^2}$

In the outer region of a self-preserving layer, δ and U_τ are the appropriate normalizing length and velocity scales. Antonia, Rajagopalan & Zhu (1996*a*) pointed out that, since $\overline{\epsilon}$ scales on δ and U_τ, the mean-square vorticity will depend not only on δ and U_τ, but also on the Reynolds number. Specifically, they argued that, in the outer region of a self-preserving layer,

$$\overline{\omega^2} = \delta^+ \frac{U_\tau^2}{\delta^2} f\left(\frac{x_2}{\delta}\right) . \tag{6.1}$$

They provided good support for this scaling, at least for $\overline{\omega_3^2}$, using data obtained from DNS of a turbulent boundary layer (Spalart 1988) and channel flow (Kim, Moin & Moser 1987; Antonia, Kim & Browne 1991) and measurements in a turbulent boundary layer (Rajagopalan & Antonia 1993). They also suggested that the components of $\overline{\omega_3^2}$, i.e. $\overline{u_{1,2}^2}$ and $\overline{u_{2,1}^2}$, should scale in a manner similar to (6.1).

Normalized distributions of $\overline{u_{i,j}^2}$ and $\overline{\omega_i^2}$ are plotted in figures 9 and 10. Both uncorrected and corrected data are shown. For comparison, the smooth wall data

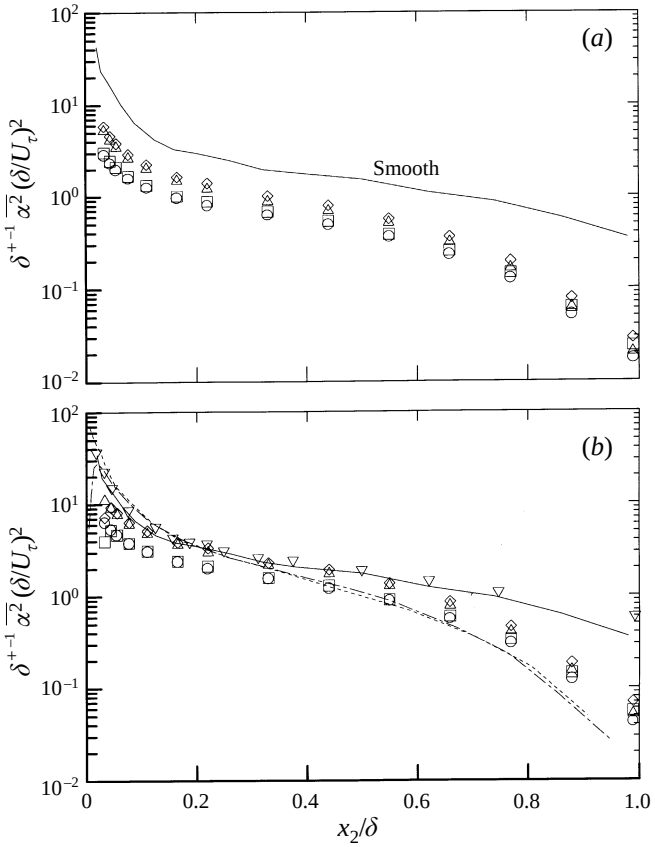

FIGURE 10. Comparison between normalized distributions of $\overline{u_{i,j}^2}$ and $\overline{\omega_i^2}$ over smooth and rough walls. Rough wall, uncorrected data : □, ○; corrected data : ◇, △. Smooth wall, all are uncorrected data. (*a*) Rough wall : □, ◇, $\alpha = u_{1,2}$; ○, △, $u_{1,3}$. Smooth wall : —, $\alpha = u_{1,2}$. (*b*) Rough wall : □, ◇, $\alpha = \omega_3$; ○, △, ω_2. Smooth wall : —, $\alpha = \omega_3$ (Rajagopalan & Antonia 1993); ▽, ω_3, $\delta^+ = 966$ (Klewicki & Falco 1990); — - —, $\alpha = \omega_3$, $\delta^+ = 651$ (Spalart 1988); - - -, ω_2 (Spalart 1988).

of Rajagopalan & Antonia (1993) for $Re_\theta = 1450$ (only $\overline{\omega_3^2}$, $\overline{u_{1,1}^2}$, $\overline{u_{2,1}^2}$ and $\overline{u_{1,2}^2}$ are available) and of Klewicki & Falco (1990) for $Re_\theta = 2870$ ($\overline{\omega_3^2}$ only) are included in the figures. These latter data are not corrected for spatial resolution.

The results indicate that the roughness affects $\overline{u_{i,j}^2}$ and $\overline{\omega_i^2}$ differently. The normalized magnitudes of $\overline{u_{1,1}^2}$ are reduced over the major part of the layer. Compared to the smooth wall data, there is a significant increase in the normalized values of $\overline{u_{2,1}^2}$ and $\overline{u_{3,1}^2}$ over the rough wall (figure 9*b*). This increase may reflect the enhancement of u_2 (and possibly u_3) activity over the rough wall. Indeed, the flow visualizations of Grass (1971) showed that violent 'ejections' and 'sweeps' occurred in a boundary layer over a gravel surface. Krogstad *et al.* (1992) found that not only are ejections (Q2 events) and sweeps (Q4 events) more intense – after normalization by U_τ^2 – in the rough wall layer but their frequency of occurrence is nearly twice as large as in a smooth wall layer. In this context, the present large values of $\delta^{+-1}\overline{u_{2,1}^2}(\delta/U_\tau)^2$ seem consistent with the documented characteristics of the Q2 and Q4 events in the layer. The present results also seem to suggest a direct link between strong and frequent Q2

and Q4 events and higher magnitudes of $\delta^{+-1}\overline{u_{3,1}^2}(\delta/U_\tau)^2$. This seems consistent with an approach towards isotropy, since $u_{2,1}$ and $u_{3,1}$ would then be perfectly correlated. Physically, it also reflects the three-dimensional nature of the surface and hence the three-dimensionality of ejections and sweeps. Note that the increase in the strength of Q2 and Q4 events is offset by an increase in the magnitude of Q1 and Q3 events since the Reynolds shear stress is constant and approximately equal to U_τ^2 in the inner layer.

The values of $\delta^{+-1/2}\overline{u_{1,2}^2}^{1/2}\delta/U_\tau$ are significantly smaller over the rough wall than over the smooth wall (figure 10*a*). This should be a direct consequence of the changes in major $u_{1,2}$-producing motions over the former wall. Experimental (e.g. Johansson & Alfredsson 1982) and numerical (Robinson 1991*b*; Johansson, Alfredsson & Kim 1987) studies have confirmed the existence of 'near-wall shear layers' over a smooth wall ($x_2^+ \leqslant 100$). These layers originate as a result of the no-slip condition at the surface and give rise to high instantaneous values of $U_{1,2}$. The magnitude of $\overline{u_{1,2}^2}$ in the wall region is, in a sense, a measure of the strength of these shear layers. It is conceivable that by relaxing the no-slip condition at the wall, due to surface roughness, both the rate of generation and strength of the shear layers may be reduced. Dubief, Djenidi & Antonia (1997) reported measurements of $\overline{u_{1,2}^{+\,2}}$ in the wall regions of turbulent boundary layers over a smooth wall and a riblet surface. Their results indicated that, relative to the smooth wall, the values of $\overline{u_{1,2}^{+\,2}}^{1/2}$ at $x_2^+ = 10$ are decreased by 15% for the drag-reducing case ($Re_\theta = 540$, $s^+ = h^+ = 17.3$; s and h are the spacing and height of the riblets respectively) and 40% for the drag-augmenting case ($Re_\theta = 940$, $s^+ = h^+ = 29.2$). The 'near-wall shear layers' are apparently weakened by the grooves; their strength may be further weakened as the roughness increases. The interaction between the inner and outer region of a rough wall layer is expected to be more intense than over a smooth wall (e.g. Krogstad *et al.* 1992; Shafi & Antonia 1995). The absence of strong shear layers near the rough wall may lead to a reduction of $\overline{u_{1,2}^2}$ in the outer region.

The influence of roughness is less marked on $\overline{\omega_i^2}$ than on $\overline{u_{i,j}^2}$. While there are differences between smooth and rough wall values of $\delta^{+-1}\overline{u_{i,j}^2}(\delta/U_\tau)^2$, the distributions of $\delta^{+-1}\overline{\omega_3^2}(\delta/U_\tau)^2$ in the two layers, shown in figure 10(*b*), appear to be similar for a major portion of the outer layer ($0.1 \leqslant x_2/\delta \leqslant 0.5$). Note that for Rajagopalan & Antonia's (1993) measurements, Δx_2^* varies from 2.7 to 1.9 in the range $0.09 \leqslant x_2/\delta \leqslant 0.5$. In view of the smaller values of Δx_2^* used by these authors, it is possible that their $\overline{\omega_3^2}$ data may have already been overestimated. Surprisingly, there is good agreement between the $\overline{\omega_3^2}$ data of Klewicki & Falco (1990) and those of Rajagopalan & Antonia (1993), despite the fact that the spatial resolutions of the probes used in the two investigations were different. For Klewicki & Falco's (1990) data, the minimum and maximum values of Δx_2^* were respectively 0.9 and 3.4. It seems likely that the 'correct' smooth wall distribution of $\delta^{+-1}\overline{\omega_3^2}(\delta/U_\tau)^2$ would lie somewhere below both smooth wall data sets. Support for this expectation is provided by the $\delta^{+-1}\overline{\omega_i^2}(\delta/U_\tau)^2$ data of Spalart (1988) for $Re_\theta = 1410$. The normalized outer-layer values of $\overline{\omega_2^2}$ and $\overline{\omega_3^2}$ are relatively larger over the rough wall.

Several conceptual models have been proposed for the coherent structures observed in a smooth-wall turbulent boundary layer (e.g. Cantwell 1981; Robinson 1991*a*). In Falco's (1991) proposal, the outer region comprises large-scale motions and typical

eddies. The characteristics of the large-scale organized motions in smooth wall layers have been investigated extensively (e.g. Kovasznay, Kibens & Blackwelder 1970; Brown & Thomas 1977; Chen & Blackwelder 1978; Antonia, Bisset & Browne 1990). Typical eddies are described as local, compact regions of vorticity concentration with a distorted vortex-ring-like shape and behaviour. Falco argued that $\overline{\omega_3^2}^{1/2}$ should provide a reliable measure of the strength of these eddies in the outer layer. The present results would then suggest that the strength of these eddies is increased by the roughness.

Falco (1991) proposed that the characteristic velocity of the typical eddies U_{TE} can be expressed as $U_{TE} = C_1\overline{\omega_3^2}^{1/2}C_{x_2}$, where C_1 is a constant (= 0.104) and C_{x_2} is the average length scale of the typical eddies. He suggested that the dependence of C_{x_2} on Re_θ can be described as $C_{x_2}/\delta = C_2 Re_\theta^{-0.758}$, where C_2 (= 30.5) is a constant. On the basis of Klewicki & Falco's (1990) ω_3 measurements, he argued that in the region $5 \leqslant x_2^+ \leqslant \delta^+$, $\overline{\omega_3^2}^{1/2} = F(x_2^+)U_\tau^2/\nu$; here F is a universal function. Using these results, he showed that $U_{TE}/U_\tau = 1.64(x_2^+)^{-0.5}Re_\theta^{0.159}$. According to Antonia *et al.* (1996*a*), $\delta^{+-1/2}\overline{\omega_3^2}^{1/2}\delta/U_\tau = f_3(x_2/\delta)$, where f_3 is a universal function, which depends on the flow. It follows that

$$U_{TE}/U_\tau = C_1\delta^{+1/2}f_3(x_2/\delta)C_{x_2}/\delta \quad . \tag{6.2}$$

Although the exact dependence of C_{x_2}/δ on Re_θ may not be known for the rough wall layer, the difference between the present distribution of $f_3(x_2/\delta)$ and that over a smooth wall suggests that the distributions of U_{TE}/U_τ would also differ in the two layers. Falco's model assumes that typical eddies are convected towards the wall by the higher-speed outer-layer fluid. This mechanism may contribute to the interaction between outer and inner regions; this interaction should be stronger over the rough wall arising from the increased strength of the typical eddies.

The present normalized distributions of both uncorrected and corrected data for $\overline{\omega_2^2}$, $\overline{u_{1,3}^2}$ and $\overline{u_{3,1}^2}$ are almost identical to those of $\overline{\omega_3^2}$, $\overline{u_{1,2}^2}$ and $\overline{u_{2,1}^2}$ respectively. This equality is not observed in the uncorrected smooth wall data (not shown) of Balint, Wallace & Vukoslavcevic (1991). Spalart's data (not shown) indicate that $\overline{\omega_2^2}^{1/2} \simeq \overline{\omega_3^2}^{1/2}$ is satisfied for $x_2/\delta > 0.1$; $\overline{\omega_1^2}^{1/2}$, $\overline{\omega_2^2}^{1/2}$ and $\overline{\omega_3^2}^{1/2}$ are approximately equal only for $x_2/\delta > 0.6$. The DNS data for a low-Reynolds-number turbulent channel flow (Antonia *et al.* 1991) indicate that the ratio $\overline{u_{1,2}^2}/\overline{u_{1,3}^2}$ approaches the value of 1 for $x_2^+ \geqslant 40$. For $\overline{u_{2,1}^2}/\overline{u_{3,1}^2}$, the rate of convergence towards 1 is slower than for $\overline{u_{1,2}^2}/\overline{u_{1,3}^2}$; $\overline{\omega_2^{+2}} \simeq \overline{\omega_3^{+2}}$ for $x_2^+ \geqslant 40$. Away from the wall, Choi, Moin & Kim's (1993) DNS data for a turbulent channel flow over riblets indicate that, in a drag-augmenting mode ($s^+ = 40$, $h^+ = 20$; s and h are the width and height of the riblet elements), $\overline{\omega_2^2} \simeq \overline{\omega_3^2}$. Since the equalities $\overline{u_{1,2}^2} = \overline{u_{1,3}^2}$, $\overline{u_{2,1}^2} = \overline{u_{3,1}^2}$ and $\overline{\omega_2^2} = \overline{\omega_3^2}$ are consistent with local axisymmetry (George & Hussein 1991), the turbulence structure in the present rough wall layer closely satisfies local axisymmetry.

Ratios of different velocity derivative and vorticity variances have been compared in the literature with isotropy. For example, the the ratios

$$K_1 \equiv 2\overline{u_{1,1}^2}/\overline{u_{2,1}^2}, \tag{6.3}$$

$$K_2 \equiv 2\overline{u_{1,1}^2}/\overline{u_{3,1}^2}, \tag{6.4}$$

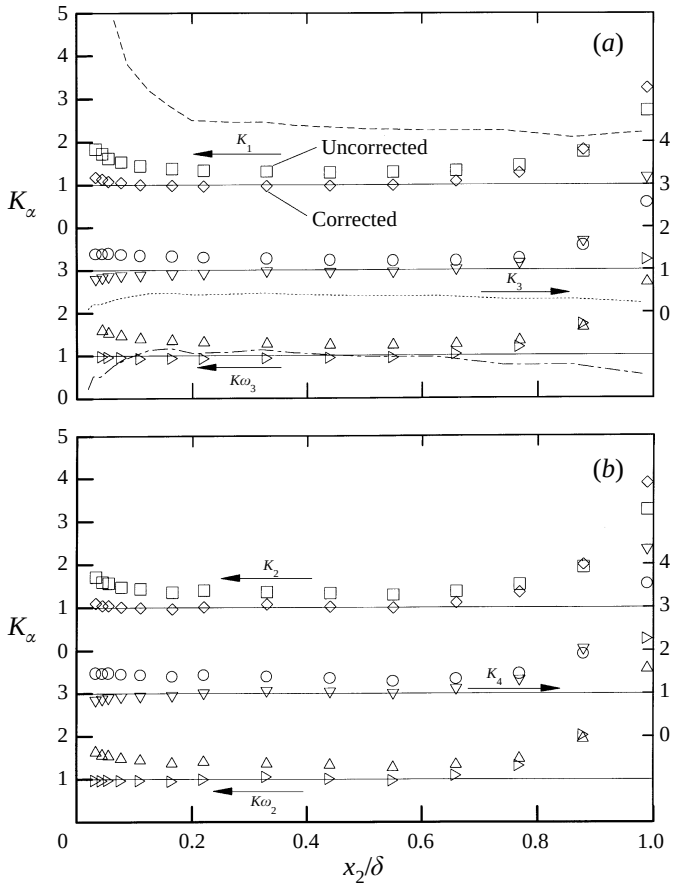

FIGURE 11. Distributions of K_1, K_2, K_3, K_4, K_{ω_3} and K_{ω_2} (equations (6.3)–(6.8)). (*a*) Rough wall, uncorrected data : □, K_1; ○, K_3; △, K_{ω_3}; corrected data : ◇, K_1; ▽, K_3; ▷, K_{ω_3}. Smooth wall, uncorrected data : - - -, K_1; ···, K_3; — - —, K_{ω_3}. (*b*) Rough wall, uncorrected data : □, K_2; ○, K_4; △ K_{ω_2}; corrected data : ◇, K_2; ▽, K_4; ▷, K_{ω_2}.

$$K_3 \equiv 2\overline{u_{1,1}^2}/\overline{u_{1,2}^2}, \tag{6.5}$$

$$K_4 \equiv 2\overline{u_{1,1}^2}/\overline{u_{1,3}^2}, \tag{6.6}$$

$$K_{\omega_2} \equiv 5\overline{u_{1,1}^2}/\overline{\omega_2^2}, \tag{6.7}$$

$$K_{\omega_3} \equiv 5\overline{u_{1,1}^2}/\overline{\omega_3^2}, \tag{6.8}$$

should be equal to 1 in isotropic turbulence.

Browne, Antonia & Shah (1987) reviewed data for K_1, K_2, K_3 and K_4 obtained in various flows. Noting that there were fewer published results for K_3 and K_4 than for K_1 and K_2, they found that $K_1 \simeq K_2 > 1$ and $K_3 \simeq K_4 < 1$. Verollet (1972) reported that $K_1 = 1.72$ and $K_2 = 1.59$ at $x_2/\delta \simeq 0.32$ in a smooth wall boundary layer. For a turbulent channel flow, Antonia *et al.* (1991) found that the magnitudes of K_1 ($\simeq 4$ at $x_2^+ = 30$), K_2 ($\simeq 2$), K_3 (0.22) and K_4 (0.22) slowly approach 1 at the centreline. The present distributions of the ratio K_α are plotted in figure 11. Both corrected and uncorrected data are shown in the figure. All the uncorrected ratios deviate significantly from the isotropic value. After correction, the distributions of the

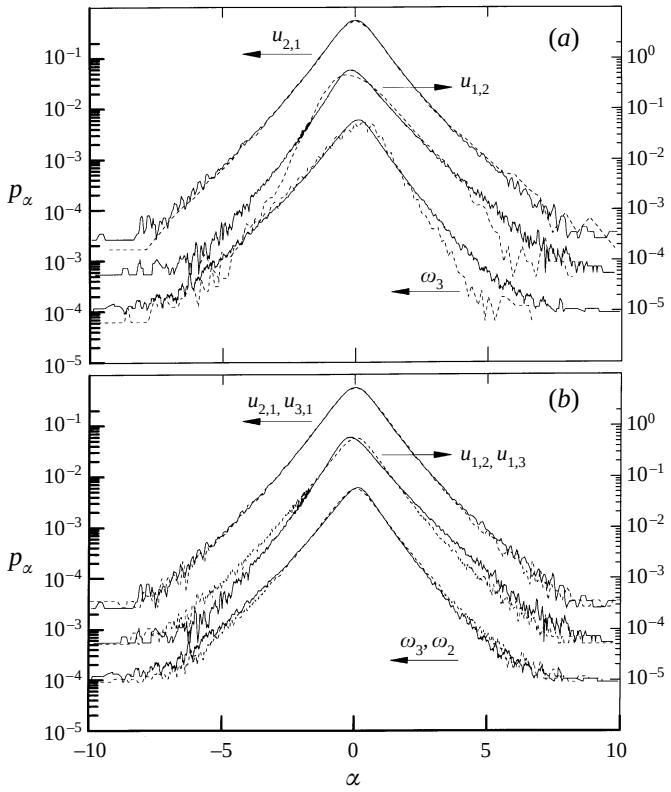

FIGURE 12. Probability density functions of $u_{i,j}$ and ω_i. (*a*) Top : $\alpha = u_{2,1}$: —, rough wall, $x_2/\delta \simeq 0.44$; - - -, smooth wall, $x_2/\delta \simeq 0.5$. Middle : $\alpha = u_{1,2}$: symbols are as in the top. Bottom : $\alpha = \omega_3$: symbols are as in the top. (*b*) Top : —, $\alpha = u_{2,1}$; - - -, $u_{3,1}$, rough wall, $x_2/\delta \simeq 0.44$. Middle : —, $\alpha = u_{1,2}$; - - -, $u_{1,3}$. Bottom : —, $\alpha = \omega_3$; - - -, ω_2.

ratios are approximately equal to 1 over a significant portion of the layer. Recalling that the corrections to spectra of $u_{i,1}$ (whose integrals with respect to k_1 yield $\overline{u_{i,1}^2}$) do not involve the assumption of isotropy, greater weighting should be given to K_1 and K_2 than to K_3 and K_4; the corrected distributions of K_{ω_2} and K_{ω_3} should also be reliable. Uncorrected values of K_1, K_3 and K_{ω_3}, inferred from smooth-wall boundary layer data (obtained from the experiment of Rajagopalan & Antonia 1993), are also included in figure 11. The magnitude of K_1 is significantly larger than 1. By contrast, K_3 is smaller than 1 everywhere in the layer, consistent with the conclusion of Browne *et al.* (1987). Interestingly, the distribution of K_{ω_3} is close to 1, possibly reflecting the compensation arising from the opposite trends of K_1 and K_3.

7. PDFs and higher-order moments

The one-point probability density functions (p.d.f.) of turbulence quantities (or p_α in short) are expected to depend on the boundary conditions or the type of flow. It is in this context that we examine the effect of roughness on p_α with $\alpha = u_{i,j}$ or ω_i. The distributions of p_α ($\alpha = u_{2,1}$, $u_{1,2}$ and ω_3) at $x_2/\delta \simeq 0.44$, smoothed using a window of five data points, are plotted in figure 12. The present data are compared with the smooth wall data (obtained from the experiment of Rajagopalan & Antonia

1993) at $x_2/\delta \simeq 0.5$. All distributions of p_α are normalized such that $\int \overline{\alpha^2}^{1/2} p_\alpha \mathrm{d}\alpha = 1$. A semilogarithmic presentation is used to emphasize the tails of p_α. For $\alpha = u_{2,1}$, no marked effect of roughness on $p_{u_{2,1}}$ can be discerned. Both distributions are distinctly non-Gaussian with long, approximately exponential, tails; for sufficiently large $|\alpha|$, p_α assumes the form $p_\alpha \sim \exp(-\beta|\alpha|)$, where β is a constant. In this respect, the shape of $p_{u_{2,1}}$ is similar to that previously reported for $p_{u_{1,1}}$ (e.g. Wyngaard & Tennekes 1970; Kuo & Corrsin 1974; Frenkiel & Klebanoff 1975; Frenkiel, Klebanoff & Huang 1979). While rough and smooth wall distributions for $\alpha = u_{1,2}$ are similar in shape, there are significant differences in the negative tails (figure 12*a*). In particular, compared to the smooth wall, there is a higher probability of finding large negative $u_{1,2}$ fluctuations over the rough wall. The shape of the present $p_{u_{1,2}}$ is similar to that reported for DNS data of isotropic turbulence (She, Jackson & Orszag 1988; Kida & Murakami 1989; Vincent & Meneguzzi 1991; Jimenez *et al.* 1993) and turbulent channel flow data (Dinavahi, Breuer & Sirovich 1995) as well as experimental wake data (Shafi, Zhu & Antonia 1997). The present distribution of $p_{u_{1,2}}$ is positively skewed. It is important to point out that we are unable to correct p_α for the effect of spatial resolution. At $x_2/\delta \simeq 0.44$, the present value of Δx_2^* is 6.2. For the smooth wall data, $\Delta x_2^* \simeq 1.9$ at $x_2/\delta \simeq 0.5$. Previous investigations (Jimenez 1994; Shafi *et al.* 1997) have indicated that the tails of the p.d.f. of $u_{1,2}$ are affected due to the finite value of Δx_2^*; the probability of finding large $|u_{1,2}|$ fluctuations decreases as Δx_2^* increases. Accordingly, the tails of the p.d.f.s of $u_{1,2}$ in figure 12(*a*) may have slightly different levels of attenuation. In addition, it has been observed that the tails of the p.d.f. of $u_{1,2}$ evolve as R_λ increases (Jimenez *et al.* 1993; Shafi *et al.* 1997). At $x_2/\delta \simeq 0.44$, $R_\lambda = 230$; for the smooth wall $R_\lambda \simeq 70$ ($x_2/\delta \simeq 0.5$). In view of the different effects of Δx_2^* and R_λ on the p.d.f. of $u_{1,2}$, it seems reasonable to suggest that the differences in the negative tails of the p.d.f.s should reflect differences in the turbulence structure between the two layers. The relative contribution of the positive tail, compared to that of the negative tail, to $\overline{u_{1,2}^2}$ is higher for the smooth wall layer. The surface roughness appears to reduce the difference between the contributions to $\overline{u_{1,2}^2}$ from positive and negative $u_{1,2}$ fluctuations. This seems consistent with an approach towards isotropy of the small-scale structure in the rough wall layer. For $\omega_3 < 0$, the distribution of p_{ω_3} is essentially the same for smooth and rough walls. There is however a higher probability of finding large positive ω_3 fluctuations in the rough wall layer and the asymmetry in p_{ω_3} is consequently reduced; for isotropic turbulence, p_{ω_i} is symmetric (Antonia *et al.* 1996*b*). The behaviour of the tails of p_α ($\alpha = u_{i,j}$ or ω_i) has been associated with the small-scale motion (e.g. Jimenez *et al.* 1993). In this respect, the present results suggest that the roughness can affect the nature of small-scale fluctuations.

Since the distributions of p_α for $\alpha = u_{1,1}$, $u_{2,1}$ and $u_{1,2}$ all possess long exponential tails, one may expect, albeit speculatively, that other components of $u_{i,j}$ would also exhibit non-Gaussian characteristics in their p.d.f.s. Indeed, the distributions of p_α for $\alpha = u_{3,1}$, and $u_{1,3}$ (figure 12*b*) also indicate noticeable departures from a Gaussian distribution. Their shape is similar to that of $p_{u_{1,1}}$ in the sense that they all possess long exponential tails. The distributions of $p_{u_{2,1}}$ and $p_{u_{3,1}}$ are nearly identical; both are symmetric with respect to the origin. In contrast to $p_{u_{1,3}}$, which is nearly symmetric, there is evident asymmetry in $p_{u_{1,2}}$. Small differences can be observed between the distributions of p_{ω_2} and p_{ω_3} (figure 12*b*); unlike p_{ω_2}, which is symmetrical, p_{ω_3} is negatively skewed. The present shapes of p_{ω_i} are similar to those observed in the wake flow (Antonia *et al.* 1996*a*). The results suggest that the p.d.f.s of other components of $u_{i,j}$, not measured here, may also exhibit an exponential-tail-like behaviour. Some

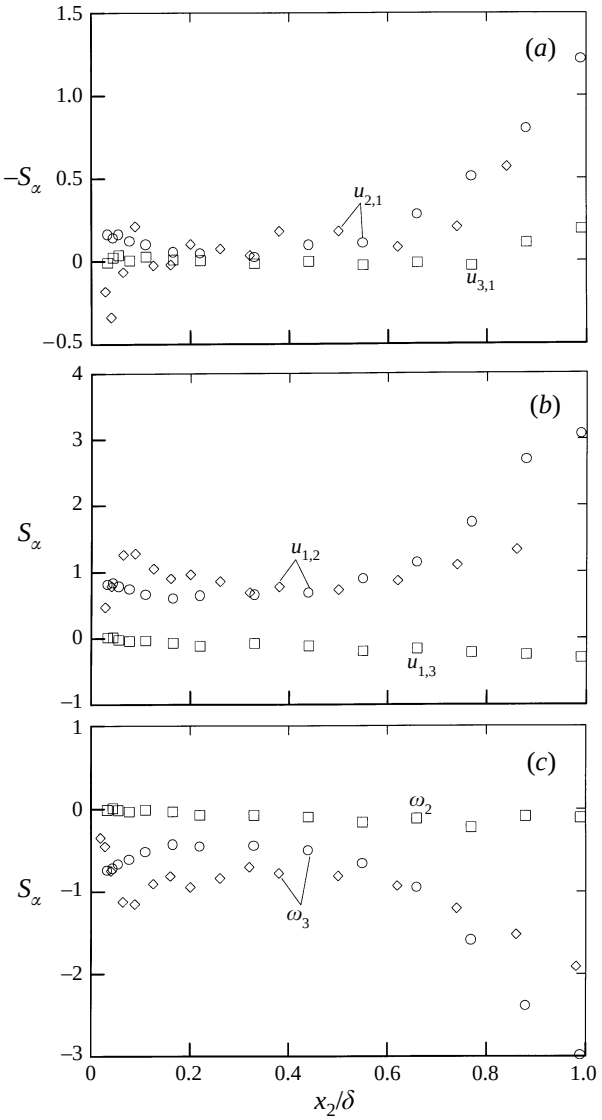

FIGURE 13. Distributions of the skewness of $u_{i,j}$ and ω_i in rough and smooth wall layers. (*a*) Rough wall : ○, $\alpha = u_{2,1}$; □, $u_{3,1}$. Smooth wall : ◇, $\alpha = u_{2,1}$. (*b*) Rough wall : ○, $\alpha = u_{1,2}$; □, $u_{1,3}$. Smooth wall : ◇, $\alpha = u_{1,2}$. (*c*) Rough wall : ○, $\alpha = \omega_3$; □, ω_2. Smooth wall : ◇, $\alpha = \omega_3$.

support for this suggestion is provided by the distribution of p_{ω_1} reported by Kida & Murakami (1989); since this distribution is exponential, $p_{u_{2,3}}$ and $p_{u_{3,2}}$ are likely to behave similarly.

Over a relatively large range ($0.1 \leqslant x_2/\delta \leqslant 0.4$), the p.d.f.s appeared to be independent of x_2/δ. This is consistent with the results of Dinavahi *et al.* (1995) who noted that, away from the near-wall region, the p.d.f.s of $u_{i,j}$ (except for $u_{1,2}$) are independent of x_2^+.

The magnitudes of the skewness S_α ($\equiv \overline{\alpha^3}/\overline{\alpha^2}^{3/2}$) and flatness factors F_α ($\equiv \overline{\alpha^4}/\overline{\alpha^2}^2$) quantify the departure of p_α from a Gaussian distribution. The distributions of S_α for $\alpha = u_{2,1}$, $u_{3,1}$, $u_{1,2}$, $u_{1,3}$, ω_3 and ω_2 are plotted in figure 13. In view of the relatively

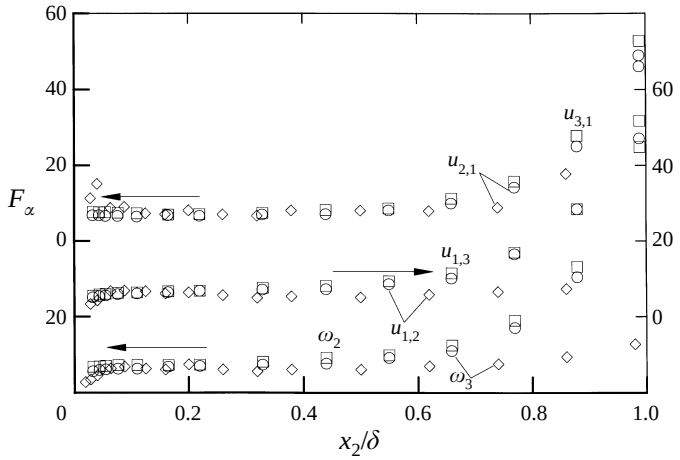

FIGURE 14. Distributions of the flatness factors of $u_{i,j}$ and ω_i. Symbols are as in figure 13.

large values of Δx_2^* (9.9 at $x_2/\delta \simeq 0.03$ to 5.1 at $x_2/\delta \simeq 0.66$), $S_{u_{1,2}}$ is expected to be underestimated. In particular, the true values of $S_{u_{1,2}}$ in the inner region will be higher than the measured data. However, we are unable to correct these data for the effect of a finite wire separation. In the range $0.05 \leqslant x_2/\delta \leqslant 0.3$, the values of $S_{u_{1,2}}$ over the rough wall are smaller than those over the smooth wall. At $x_2/\delta \simeq 0.1$, the difference is as large as 60%.

With regard to the sign of $S_{u_{1,2}}$, Tavoularis & Corrsin (1981) suggested, using a mixing-length type model, that

$$\text{sgn } S_{u_{1,2}} = \text{sgn } \overline{U}_{1,2} \, .$$

They found support for this argument from their $S_{u_{1,2}}$ ($\simeq 0.62$) data for a quasi-homogeneous shear flow with a constant value of $\overline{U}_{1,2}$. Pumir & Shraiman's (1995) numerical investigation of homogeneous shear flows suggested that a positive value of $S_{u_{1,2}}$ (0.85) reflects the effect of a uniform shear on homogeneous turbulence. A positive value of $S_{u_{1,2}}$ was also reported by Antonia *et al.* (1993) for turbulent channel flows. It appears that the influence of $\overline{U}_{1,2}$ on $S_{u_{1,2}}$ is as important in wall-bounded shear flows as in homogeneous shear flows. Although the non-zero value of the temperature derivative skewness has been attributed to the presence of coherent ramp-like features (e.g. Antonia *et al.* 1986; Sreenivasan 1991), such signatures could not be clearly distinguished in the present $u_{1,2}$ signals.

Relative to the smooth wall, the magnitude of S_{ω_3} is significantly reduced in the region $0.1 \leqslant x_2/\delta \leqslant 0.5$ over the rough wall (figure 13*c*). This trend is consistent with the differences observed in the p.d.f.s of ω_3 in figure 12(*a*). Balint *et al.* (1991) attributed the negative values of S_{ω_3} to the spanwise vortex stretching. The smaller values of both S_{ω_3} and $S_{u_{1,2}}$ indicate that the turbulence structure is closer to isotropy over the rough wall. Because of symmetry in the x_3 direction, S_{ω_2}, $S_{u_{1,3}}$ and $S_{u_{3,1}}$ should be zero. This is indeed the case for the present experiment. Also, $S_{u_{2,1}}$ is nearly zero for $x_2/\delta \lesssim 0.7$.

The distributions of F_α appear to be relatively less affected by the change in surface condition (figure 14). In both experiment (Shafi *et al.* 1996) and numerical work (Jimenez 1994) $F_{u_{1,2}}$ may depend on the choice of Δx_2^*. In particular, $F_{u_{1,2}}$ may be underestimated for large Δx_2^*. Moreover, there is a moderate dependence of $F_{u_{1,2}}$ on

R_λ, the magnitude of $F_{u_{1,2}}$ increasing with R_λ. Allowing for the difference in the value of Δx_2^* between the two layers, it is probable that the 'true' value of $F_{u_{1,2}}$ will be larger over the rough wall. However, it would be hard to assert unambiguously that this difference is solely due to the roughness since R_λ is also different between the two layers. For $x_2/\delta \leqslant 0.05$, the trend of the data suggests that the 'true' $F_{u_{1,2}}$ will be significantly higher in the rough wall layer.

8. Approximations of $\bar{\epsilon}$ and $\overline{\omega_i^2}$

Accurate estimates of the average energy dissipation rate $\bar{\epsilon}$ ($\equiv \nu\overline{u_{i,j}+u_{j,i}}$) are important in turbulence research. Since the measurement of the twelve terms which appear in the expression for $\bar{\epsilon}$ is a formidable experimental task, many attempts have been made to estimate $\bar{\epsilon}$ approximately. The easiest and most commonly used approximation assumes isotropy, namely

$$\bar{\epsilon}_I = 15\nu\overline{u_{1,1}^2}\,. \tag{8.1}$$

Wygnanski & Fiedler (1969) measured nine terms of $\bar{\epsilon}$ in a self-preserving circular jet and suggested a 'semi-isotropic' expression for $\bar{\epsilon}$,

$$\bar{\epsilon}_{SI} \simeq \nu\left[\overline{u_{1,1}^2}\,(1+4/K_1) + \overline{u_{1,2}^2}(4+K_1)\right] \tag{8.2}$$

where K_1 is defined in (6.3). When K_1 assumes the isotropic value of 1, (8.2) reduces to (8.1). Browne *et al.* (1987) measured nine terms of $\bar{\epsilon}$ in the self-preserving region of a cylinder wake. They suggested a reasonable approximation to $\bar{\epsilon}$, assuming isotropy, is

$$\bar{\epsilon} \simeq 3\nu[\overline{u_{1,1}^2} + \overline{u_{1,2}^2} + \overline{u_{1,3}^2}]\quad. \tag{8.3}$$

Using DNS data for a turbulent channel flow, Antonia *et al.* (1991) suggested an empirical formula for estimating $\bar{\epsilon}$, i.e.

$$\bar{\epsilon} \simeq \nu[2\overline{u_{1,2}^2} + 11\overline{u_{1,1}^2}]\,. \tag{8.4}$$

There are other approximations to $\bar{\epsilon}$ which are based on the assumption of axisymmetry (e.g. George & Hussein 1991; Antonia *et al.* 1991). Since these approximations require estimates of quantities (e.g. $\overline{u_{3,2}^2}$, $\overline{u_{2,3}^2}$, $\overline{u_{2,2}^2}$) that are relatively difficult to measure, they will not be considered here. Expressions (8.2)–(8.4) are particularly attractive from an experimental viewpoint. If these approximations provide reasonable estimates of $\bar{\epsilon}$, the use of only two parallel wires would then be sufficient for the purpose of measuring $\bar{\epsilon}$ in shear flows. Klebanoff (1955) measured $\overline{u_{1,1}^2}$, $\overline{u_{2,1}^2}$, $\overline{u_{3,1}^2}$, $\overline{u_{1,2}^2}$ and $\overline{u_{1,3}^2}$ in a smooth-wall boundary layer. Assuming isotropy for the rest of the terms in $\bar{\epsilon}$, he estimated $\bar{\epsilon}$ using the relation

$$\bar{\epsilon} \simeq \nu\left[\overline{u_{1,1}^2} + \overline{u_{2,1}^2} + \overline{u_{3,1}^2} + \tfrac{5}{2}(\overline{u_{1,2}^2} + \overline{u_{1,3}^2})\right]\,. \tag{8.5}$$

Another possibility is to approximate $\bar{\epsilon}$ by (e.g. Hinze 1975)

$$\bar{\epsilon} \simeq \nu[7\overline{u_{1,1}^2} + \overline{u_{2,1}^2} + \overline{u_{3,1}^2} + \overline{u_{1,2}^2} + \overline{u_{1,3}^2}]\,. \tag{8.6}$$

The universal equilibrium hypothesis of Kolmogorov (1941) suggests that, in the inertial subrange, ϕ_{u_1} has the form

$$\phi_{u_1}(k_1) = C_1\bar{\epsilon}^{2/3}k_1^{-5/3}\,. \tag{8.7}$$

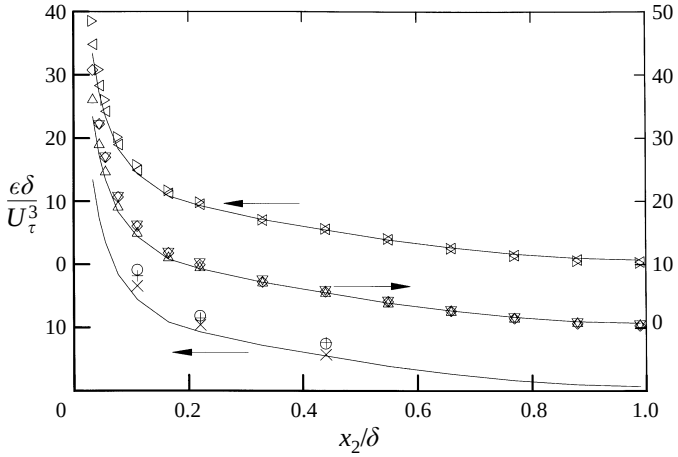

FIGURE 15. Comparison between different approximations to $\bar{\epsilon}$. —, equation (8.1); ∇, (8.2); $\diamond$, (8.3); $\triangle$, (8.4); $\triangleright$, (8.5); $\triangleleft$, (8.6); $\circ$, (8.7); $+$, (8.8); $\times$, (8.9). For clarity, the data are split into three separate groups with offset origins (the same solid line is shown in each group).

Bradshaw (1969) showed that reasonable estimates of $\bar{\epsilon}$ can be inferred from (8.7). He suggested that $C_1 \simeq 0.55$ in the outer region and $C_1 \simeq 0.51$ in the inner region of wall shear flows.

Independent estimates of $\bar{\epsilon}$ can also be obtained from the behaviour of the velocity structure functions $\overline{[\Delta u_1(r)]^n} \equiv \overline{[u_1(x+r)-u_1(x)]^n}$ for $n = 2$ and 3 in the inertial range. Kolmogorov (1941) proposed that in the inertial range

$$\overline{[\Delta u_1(r)]^2} = C_2 \bar{\epsilon}^{2/3} r^{2/3} . \tag{8.8}$$

A value of 2 for C_2 appears to be reasonably supported experimentally (e.g. Yaglom 1981). The behaviour of the third-order velocity structure function is given by (e.g. Monin & Yaglom 1975)

$$\overline{[\Delta u_1(r)]^3} = -C_3 \bar{\epsilon} r \tag{8.9}$$

where C_3 has a theoretical value of $4/5$.

Distributions of $\bar{\epsilon}\ \delta/U_\tau^3$ estimated using (8.1)–(8.6) are shown in figure 15. Corrected data for $\overline{u_{1,1}^2}$, $\overline{u_{2,1}^2}$, $\overline{u_{3,1}^2}$, $\overline{u_{1,2}^2}$ and $\overline{u_{1,3}^2}$ are used. A value of 1 is used for K_1 in (8.2). There is good agreement between different approximations of $\bar{\epsilon}$ for a significant portion of the layer. This is consistent with the distributions of K_α (figure 11). For $x_2/\delta < 0.1$, there are discrepancies between different estimates of $\bar{\epsilon}$. This is particularly evident at $x_2/\delta \simeq 0.03$ where the assumption of isotropy is untenable. Overall, for the region away from the wall, the present results provide encouraging support for $\bar{\epsilon}_I$ as a reasonable approximation to $\bar{\epsilon}$ in the present flow.

Values of $\bar{\epsilon}$ inferred from (8.7), (8.8) and (8.9) at $x_2/\delta \simeq 0.11$, 0.22 and 0.44 are also shown in figure 15. For the present $\phi_{u_1}^*(k_1^*)$ data, there exists an approximate $-5/3$ inertial range in the region $0.02 \leqslant k_1^* \leqslant 0.08$. The magnitude of C_1 estimated from the plateau in $k_1^{*5/3}\phi_u^*(k_1^*)$ is 0.67. This value is significantly larger than the atmospheric surface layer value of 0.5 reported by Kaimal *et al.* (1972) and that suggested by Sreenivasan (1996). However, it is within the range of values of C_1 reviewed by Yaglom (1981). At $x_2/\delta \simeq 0.44$, the value of $\bar{\epsilon}\ \delta/U_\tau^3$ inferred from (8.7) is 26% larger than that obtained from the isotropic estimates. The magnitude of $\bar{\epsilon}\ \delta/U_\tau^3$ obtained

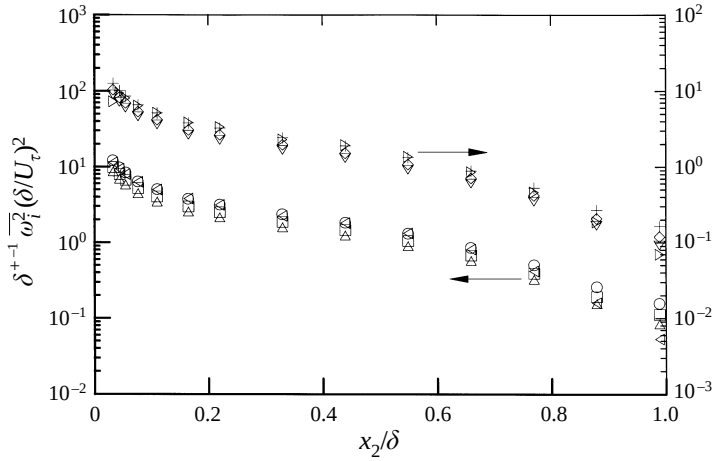

FIGURE 16. Comparison between different approximations to $\overline{\omega_i^2}$. $\triangleright$, $i = 3$, corrected data; $\triangledown$, $\alpha = 1.4$, equation (8.10); $\diamond$, 2; $+$, 3. $\triangleleft$, $i = 2$, corrected data; $\triangle$, $\alpha = 1.4$, equation (8.11); $\square$, 2; $\circ$, 3.

from (8.8) with $C_2 = 2$ is also larger. Better agreement is observed between the values of $\overline{\epsilon}\,\delta/U_\tau^3$ calculated using (8.9) and those inferred from the isotropic approximations.

Rajagopalan & Antonia (1993) approximated $\overline{\omega_3^2}$ by the expression

$$\overline{\omega_3^2} \simeq \overline{u_{1,2}^2} + \alpha \overline{u_{1,1}^2}\,. \tag{8.10}$$

They found that $\alpha = 1.4$ provided good agreement between the approximation and their measurements of $\overline{\omega_3^2}$ in the outer region. They suggested that the value of α may depend on the Reynolds number and the type of flow. Using DNS data of a fully developed turbulent channel flow, Antonia *et al.* (1991) found that $\alpha = 2$ provided satisfactory results at two Reynolds numbers ($h^+ = 180$ and 395; h is the channel half-width). This value of α also provided good approximations to $\overline{\omega_2^2}$ using a relation similar to (8.10), namely

$$\overline{\omega_2^2} \simeq \overline{u_{1,3}^2} + \alpha \overline{u_{1,1}^2}\,. \tag{8.11}$$

If local isotropy is satisfied, the value of α in (8.10) and (8.11) should be 3.

Figure 16 contains distributions of the approximated $\overline{\omega_3^2}$ (equation (8.10)) and $\overline{\omega_2^2}$ (equation (8.11)) using corrected data for $\overline{u_{1,1}^2}$, $\overline{u_{1,2}^2}$ and $\overline{u_{1,3}^2}$. Three different values of α (= 1.4, 2 and 3) are considered. Also plotted are corrected data for $\overline{\omega_3^2}$ and $\overline{\omega_2^2}$. For $\alpha = 1.4$ and 2, both (8.10) and (8.11) underestimate the values of $\overline{\omega_i^2}$. Good agreement is obtained between the corrected data and the approximations when $\alpha = 3$ in the region $x_2/\delta \geqslant 0.05$. The results suggest that isotropy-based approximations should provide accurate estimates of $\overline{\omega_i^2}$ for a substantial portion of the present rough wall layer. It therefore seems reasonable to expect that other velocity derivatives – not measured in the present experiment – should also satisfy isotropy. Consequently, one should be able to estimate $\overline{\omega_1^2}$ and $\overline{\omega^2}$ with reasonable accuracy. The inferred distribution of $\delta^{+-1}\overline{\omega^2}(\delta/U_\tau)^2$ for the present flow is shown in figure 17. Here $\overline{\omega^2}$ is approximated using $\overline{\omega^2} \simeq \overline{\omega_3^2} + 2\overline{\omega_2^2}$; note that the approximation $\overline{\omega^2} \simeq 3\overline{\omega_2^2} \simeq 3\overline{\omega_3^2}$ would have yielded identical results. The smooth wall data of Spalart (1988) are also shown in the figure. Spalart's data suggest that, in the smooth wall outer layer,

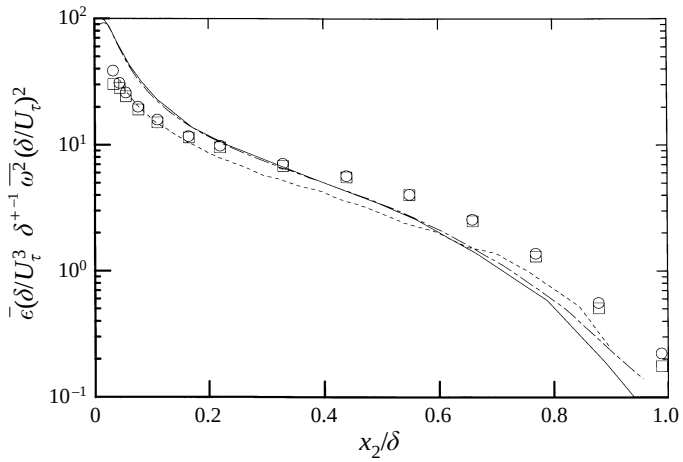

FIGURE 17. Comparison between the normalized approximations to $\overline{\omega^2}$ and $\bar{\epsilon}$ in the rough and smooth wall layers. Rough wall : □, $\overline{\omega^2}$, approximated as $\overline{\omega_3^2} + 2\overline{\omega_2^2}$ (this is essentially equivalent to $3\overline{\omega_2^2}$ or $3\overline{\omega_3^2}$); ○, $\bar{\epsilon}$, equation (8.5). Smooth wall : —, $\overline{\omega^2}$; — - —, $\bar{\epsilon}$ (Spalart 1988); - - -, $\bar{\epsilon}$ (Klebanoff 1955).

$\delta^{+-1}\overline{\omega^2}(\delta/U_\tau)^2$ is smaller than in the rough wall layer. The present distribution of $\delta^{+-1}\overline{\omega^2}(\delta/U_\tau)^2$ is identical to that of $\bar{\epsilon}\ \delta/U_\tau^3$, obtained using (8.5). This conforms with the assumption of homogeneity, i.e. $\bar{\epsilon} = \nu\overline{\omega^2}$. Compared to the smooth wall values of $\bar{\epsilon}\ \delta/U_\tau^3$ of Klebanoff (1955) and Spalart (1988), the present values are larger in the outer region of the flow (figure 16), consistent with the increased production of turbulent kinetic energy in the rough wall layer.

The increase in $\delta^{+-1}\overline{\omega^2}(\delta/U_\tau)^2$ and $\bar{\epsilon}\delta/U_\tau^3$ in the rough wall is not as large as that previously observed for most components of the Reynolds stress tensor. There is a hint here that vorticity-producing motions may not be the only Reynolds-stress-producing mechanism in the outer layer. For example, strong Reynolds-stress-producing ejections (or Q2 events) originating from the wall region may extend well into the outer layer. Stronger large-scale motions (Krogstad & Antonia 1994) would also contribute to the Reynolds stress production. It seems appropriate to comment briefly on the possible Reynolds-stress-producing motion in the inner region of the rough wall layer. Quasi-streamwise vortical structures are usually assumed to be the major structural element responsible for turbulence production in the near-wall region of a smooth-wall boundary layer (e.g. Robinson 1991*b*; Bernard, Thomas & Handler 1993). In this region, 'low-speed streaks' are often believed to be generated by the passage of these structures over the smooth wall. Intuitively, one would not expect these structures to survive over the present mesh roughness. This expectation is supported by the reduced anisotropy of the Reynolds stresses (Shafi & Antonia 1995). An alternative mechanism, which may play an important role in the turbulence production in the inner region, is the creation of wakes by the roughness elements. Bandyopadhyay (1987) speculated that the quasi-cyclic nature of these wakes may determine momentum and heat transports from the wall. A further possibility relates to the existence of a reservoir of low-speed fluid in the interstices between roughness elements. The ejection of this fluid away from the wall may occur violently, possibly through the interaction with relatively intense wall-ward sweep-like motions. Such a

scenario would be consistent with strong values of $-\overline{u_1^+ u_2^+}$, though not necessarily strong $\overline{\omega^2}$, in the inner region.

9. Conclusions

Measurements of the spanwise and wall-normal components of vorticity (ω_2 and ω_3) have been made in the fully developed turbulent boundary layer over a mesh-screen roughness with a four-hot-wire vorticity probe. The measured spectra of ω_2 and ω_3 and their constituent velocity derivatives were corrected for the spatial resolution of the probe and compared with the relevant isotropic expressions. There is support for isotropy at high wavenumbers, in particular, from spectra of $u_{2,1}$ and $u_{3,1}$. The wavenumber at which vorticity spectra conform with local isotropy was found to be $k_1(\bar{\epsilon}/S^3)^{1/2} \simeq 1$, which is significantly smaller than that ($\simeq 15$) for $u_1 u_2$ cospectra. Additional support for isotropy is provided by the values of the ratios K_1–K_4, K_{ω_2} and K_{ω_3}; they are all close to the isotropic value of 1.

Surface roughness appears to affect the elements of $\overline{u_{i,j}^2}$ and $\overline{\omega_i^2}$ differently. In particular, compared to the smooth wall values, the magnitudes of $\delta^{+-1}\overline{u_{i,j}^2}(\delta/U_\tau)^2$ for $i = 2$ and $j = 1$ are significantly increased in the rough wall layer, consistent with the presence of stronger and more frequent ejections and sweeps. On the other hand, the magnitude of $\delta^{+-1}\overline{u_{1,2}^2}(\delta/U_\tau)^2$ is reduced markedly over the rough wall, apparently reflecting the reduced strength and frequency of near-wall shear layers. Overall, the effect of the roughness is less pronounced in $\overline{\omega_i^2}$ than in $\overline{u_{i,j}^2}$. The present data indicate a relatively moderate increase of $\delta^{+-1}\overline{\omega_i^2}(\delta/U_\tau)^2$ for $i = 2$ and 3 in the outer layer, suggesting the presence of somewhat stronger vortical motions in this region.

Additional differences between smooth and rough wall layers can be observed in the p.d.f.s of $u_{1,2}$ and ω_3. Although the shapes of $p_{u_{1,2}}$ and p_{ω_3} are similar in both layers, large negative fluctuations of $u_{1,2}$ and large positive ω_3 fluctuations are more probable over the rough wall. Further, the asymmetries in both $p_{u_{1,2}}$ and p_{ω_3} are reduced in the rough wall layer. Correspondingly, the magnitudes of the skewnesses $S_{u_{1,2}}$ and S_{ω_3} are smaller over the rough wall.

Different approximations to $\bar{\epsilon}$ and $\overline{\omega_i^2}$ have been considered. The results suggest that, outside the wall region, reasonable estimates of $\bar{\epsilon}$ and $\overline{\omega_i^2}$ can be obtained by assuming isotropy. In the outer region, the inferred values of $\delta^{+-1}\overline{\omega^2}(\delta/U_\tau)^2$ are relatively larger over the rough wall than on the smooth wall, apparently implying increased vortex stretching in the rough wall layer.

The present results indicate that the surface roughness has a marked effect on the small-scale structure throughout the layer. Different small-scale quantities are affected differently but the overall effect is an unquestionable tendency towards isotropy. This feature should be useful in the context of developing $k-\epsilon$ and Reynolds stress models as well as large-eddy simulations for a turbulent boundary layer over a roughness similar to that considered here. The results also confirm that there are important differences in turbulence structure between the present rough-wall boundary layer and a smooth wall layer. Although the present roughness is classified as 'k-type', this classification is based solely on the effect the roughness has on the logarithmic mean velocity profile and is inappropriate for characterizing the Reynolds stresses or, more generally, the turbulence structure; we believe there is enough evidence, including the recent rough wall data of Westbury (1996), to support this contention. The degree of isotropy exhibited by the present rough wall layer may not apply to boundary layers

over other k-type rough walls. The three-dimensionality of the roughness, perhaps quantifiable through the roughness aspect ratio considered by Bandyopadhyay & Watson (1988), may play a major role in determining the degree of anisotropy of both large-scale and small-scale structures in the layer. It is recommended that the small-scale structure in boundary layers over other k-type rough walls, preferably with significantly different roughness aspect ratios, be examined in the same detail as in the present study.

The support of the Australian Research Council is gratefully acknowledged. The authors are grateful to Drs S. Rajagopalan and Y. Zhu for their contributions to various aspects of this work.

REFERENCES

Antonia, R. A., Anselmet, F. & Chambers, A. J. 1986 Assessment of local isotropy using measurements in a turbulent plane jet. *J. Fluid Mech.* **163**, 365–391.

Antonia, R. A., Bisset, D. K. & Browne, L. W. B. 1990 Effect of Reynolds number on the topology of the organized motion in a turbulent boundary layer. *J. Fluid Mech.* **213**, 267–286.

Antonia, R. A., Browne, L. W. B. & Shah, D. A. 1988 Characteristics of vorticity fluctuations in a turbulent wake. *J. Fluid Mech.* **189**, 349–365.

Antonia, R. A. & Kim, J. 1994 A numerical study of local isotropy of turbulence. *Phys. Fluids* A **6**, 834–841.

Antonia, R. A., Kim, J. & Browne, L. W. B. 1991 Some characteristics of small-scale turbulence in a turbulent duct flow. *J. Fluid Mech.* **233**, 369–388.

Antonia, R. A. & Mi, J. 1993 Temperature dissipation in a turbulent round jet. *J. Fluid Mech.* **250**, 531–551.

Antonia, R. A., Rajagopalan, S. & Zhu, Y. 1996*a* Scaling of mean square vorticity in turbulent flows. *Expts. Fluids* **20**, 393–394.

Antonia, R. A. & Raupach, M. R. 1993 Spectral scaling in a high Reynolds number laboratory boundary layer. *Boundary-layer Met.* **65**, 289–306.

Antonia, R. A., Satyaprakash, B. R. & Hussain, A. K. M. F. 1982 Statistics of fine-scale velocity in turbulent plane and circular jets. *J. Fluid Mech.* **119**, 55–89.

Antonia, R. A., Teitel, M., Kim, J. & Browne, L. W. B. 1992 Low Reynolds number effects in a fully developed turbulent duct flow. *J. Fluid Mech.* **236**, 579–605.

Antonia, R. A., Zhu, Y. & Kim, J. 1993 On the measurement of lateral velocity derivatives in turbulent flows. *Expts. Fluids* **15**, 65–69.

Antonia, R. A., Zhu, Y. & Shafi, H. S. 1996*b* Lateral vorticity measurements in a turbulent wake. *J. Fluid Mech.* **323**, 173–200.

Balint, J-L., Wallace, J. M. & Vukoslavcevic, P. 1991 The velocity and vorticity vector fields of a turbulent boundary layer. Part 2. Statistical properties. *J. Fluid Mech.* **228**, 53–86.

Bandyopadhyay, P. R. 1987 Rough-wall turbulent boundary layers in the transition regime. *J. Fluid Mech.* **180**, 231–266.

Bandyopadhyay, P. R. & Watson, R. D. 1988 Structure of rough-wall turbulent boundary layers. *Phys. Fluids* **31**, 1877–1883.

Batchelor, G. K. 1953 *The Theory of Homogeneous Turbulence*. Cambridge University Press.

Bernard, P. S., Thomas, J. M. & Handler, R. A. 1993 Vortex dynamics and the production of Reynolds stress. *J. Fluid Mech.* **253**, 385–419.

Bradshaw, P. 1969 Conditions for the existence of an inertial subrange in turbulent flow, *NPL Aero Rep.* 3603. Aeronautical Research Council.

Brown, G. L. & Thomas, A. S. W. 1977 Large structure in a turbulent boundary layer. *Phys. Fluids* **20**, S243–S2152.

Browne, L. W. B., Antonia, R. A. & Chambers, A. J. 1983 Effects of the separation between cold wires on the spatial derivatives of temperature in a turbulent flow. *Boundary-Layer Met.* **27**, 129–139.

Browne, L. W. B., Antonia, R. A. & Chua, L. P. 1989 Calibration of X-probes for turbulent flow measurements. *Expts. Fluids* **7**, 201–208.

Browne, L. W. B., Antonia, R. A. & Shah, D. A. 1987 Turbulent energy dissipation in a wake. *J. Fluid Mech.* **179**, 307–326.

Cantwell, B. J. 1981 Organized motion in turbulent flow. *Ann. Rev. Fluid Mech.* **13**, 457–515.

Champagne, F. H., Sleicher, C. A. & Wehrmann, O. H. 1967 Turbulence measurements with inclined hot wires. Part 1. Heat transfer experiments with inclined hot wires. *J. Fluid Mech.* **28**, 153–175.

Chen, C. H. P. & Blackwelder, R. F. 1978 Large-scale motion in a turbulent boundary layer : A study using temperature contamination. *J. Fluid Mech.* **89**, 1–31.

Choi, H., Moin, P. & Kim, J. 1993 Direct numerical simulation of turbulent flow over riblets. *J. Fluid Mech.* **255**, 503–539.

Corrsin, S. 1958 On local isotropy in a turbulent shear flow. *NACA Rep.* 58B11.

Corrsin, S. & Kistler, A. L. 1955 Free-stream boundaries of turbulent flows. *NACA Rep.* 1244.

Dinavahi, S. P. G., Breuer, K. S. & Sirovich, L. 1995 Universality of probability density functions in turbulent channel flow. *Phys. Fluids* **7**, 1122–1129.

Dubief, Y., Djenidi, L. & Antonia, R. A. 1997 The measurement of $\partial u/\partial y$ in a turbulent boundary layer over a riblet surface. *Intl J. Heat Fluid Flow* **18**, 183–187.

Durbin, P. A. & Speziale, C. G. 1991 Local anisotropy in strained turbulence at high Reynolds numbers. *Trans ASME: J. Fluids Engng* **113**, 707–709.

Elavarasan, R., Djenidi, L. & Antonia, R. A. 1996 A check of Taylor's hypothesis using two-point LDV measurements in a turbulent boundary layer. In *Proc. Eighth Symposium on Application of Laser Techniques to Fluid Mechanics, Lisbon* (ed. R. J. Adrian, D. F. G. Durão, F. Durst, M. V. Heitor, M. Maeda and J. H. Whitelaw), Vol. 2, pp. 29.1.2–29.1.5.

Ewing, D., Hussein, H. J. & George, W. K. 1995 Spatial resolution of parallel hot-wire probes for derivative measurements. *Exptl Therm. Fluids Sci.* **11**, 155–173.

Falco, R. E. 1991 A coherent structure model of the turbulent boundary layer and its ability to predict Reynolds number dependence. *Phil. Trans. R. Soc. Lond.* A **336**, 103–129.

Fan, M. S. 1991 Features of vorticity in fully turbulent flows. PhD Thesis, Yale University.

Folz, A. B. 1993 Vorticity and drag measurements in rough-wall turbulent boundary layers. MSc Thesis, Department of Mechanical Engineering, Michigan State University.

Foss, J. F. 1979 Transverse vorticity measurements. In *Proc. Dynamics Flow Conference 1978, Skovlunde, DISA* (ed. B. W. Hansen), pp. 983–1001.

Foss, J. F., Ali, S. K. & Haw, R. C. 1987 A critical analysis of transverse vorticity measurements in a large plane shear layer. In *Advances in Turbulence* (ed. G. Comte-Bellot and J. Mathieu), pp. 446–455. Springer.

Frenkiel, F. N. & Klebanoff, P. S. 1975 On lognormality of small-scale structure of turbulence. *Boundary-Layer Met.* **8**, 173–200.

Frenkiel, F. N., Klebanoff, P. S. & Huang, T. 1979 Grid turbulence in air and water. *Phys. Fluids* **22**, 1606–1617.

George, W. K. & Hussein, H. J. 1991 Locally axisymmetric turbulence. *J. Fluid Mech.* **233**, 1–23.

Grass, A. J. 1971 Structural features of turbulent flow over smooth and rough boundaries. *J. Fluid Mech.* **50**, 233–255.

Hama, F. R. 1954 Boundary layer characteristics for smooth and rough surfaces. *Trans. Soc. Naval Archit. Marine Engrs* **62**, 333–358.

Haw, R. C., Foss, J. K. & Foss, J. F. 1989 Vorticity based intermittency measurements in a single stream shear layer. In *Advances in Turbulence II* (ed. H. H. Fernholz and H. E. Fiedler), pp. 90–95. Springer.

Hinze, J. O. 1975 *Turbulence*. McGraw-Hill.

Jimenez, J. 1994 Resolution requirements for velocity gradients in turbulence. *Annual Research Briefs*, pp. 357–364. Center for Turbulence Research, NASA-Ames and Stanford University.

Jimenez, J., Wray, A. L., Saffman, P. G. & Rogallo, R. S. 1993 The structure of intense vorticity in isotropic turbulence. *J. Fluid Mech.* **255**, 65–90.

Johansson, A. V. & Alfredsson, P. H. 1982 On the structure of turbulent channel flow. *J. Fluid Mech.* **122**, 295–314.

Johansson, A. V., Alfredsson, P. H. & Kim, J. 1987 Shear-layer structures in near-wall turbulence. *Proc. Summer Program*. Center for Turbulence Research, NASA-Ames and Stanford University.

Kaimal, J. C., Wyngaard, J. C., Izumi, Y. & Coté, O. R. 1972 Spectral characteristics of surface-layer turbulence. *Q. J. R. Met. Soc.* **98**, 563–589.

Kida, S. & Murakami, Y. 1989 Statistics of velocity gradients in turbulence at moderate Reynolds number. *Fluid Dyn. Res.* **4**, 347–370.

Kim, J. & Antonia, R. A. 1993 Isotropy of the small scales of turbulence at low Reynolds number. *J. Fluid Mech.* **251**, 219–238.

Kim, J. & Hussain, F. 1992 Propagation velocity and space-time correlation of perturbations in turbulent channel flow. *NASA Tech. Mem.* 103932. NASA-Ames Research Center.

Kim, J., Moin, P. & Moser, R. 1987 Turbulence statistics in a fully developed channel flow at low Reynolds number. *J. Fluid Mech.* **177**, 133–166.

Klebanoff, P. S. 1955 Characteristics of turbulence in a boundary layer with zero pressure gradient. *NACA Rep.* 1247.

Klewicki, J. C. & Falco, R. E. 1990 On accurately measuring statistics associated with small-scale structure in turbulent boundary layers using hot-wire probes. *J. Fluid Mech.* **219**, 119–142.

Klewicki, J. C., Falco, R. E. & Foss, J. F. 1992 Some characteristics of the vortical motions in the outer region of turbulent boundary layers. *Trans ASME J. Fluids Engng* **114**, 530–536.

Kolmogorov, A. N. 1941 Local structure of turbulence in an incompressible fluid for very large Reynolds numbers. *Dokl. Akad. Nauk. SSSR.* **30**, 299–303.

Kovasznay, L. S. G., Kibens, V. & Blackwelder, R. F. 1970 Large scale motions in the intermittent region of a turbulent boundary layer. *J. Fluid Mech.* **41**, 283–325.

Krogstad, P-Å. & Antonia, R. A. 1994 Structure of turbulent boundary layers on smooth and rough walls. *J. Fluid Mech.* **277**, 1–21.

Krogstad, P-Å., Antonia, R. A. & Browne, L. W. B. 1992 Comparison between rough and smooth-wall turbulent boundary layers. *J. Fluid Mech.* **245**, 599–617.

Kuo, A. Y. & Corrsin, S. 1971 Experiments on internal intermittency and fine structure distribution functions in fully turbulent fields. *J. Fluid Mech.* **50**, 285–319.

Lee, J. M., Kim, J. & Moin, P. 1990 Structure of turbulence at high shear rate. *J. Fluid Mech.* **216**, 561–583.

Mestayer, P. 1982. Local isotropy and anisotropy in a high-Reynolds number turbulent boundary layer. *J. Fluid Mech.* **125**, 475–503.

Mestayer, P. & Chambaud, P. 1979 Some limitations to measurements of turbulence micro-structure with hot and cold wires. *Boundary-Layer Met.* **16**, 311–329.

Mi, J. & Antonia, R. A. 1996 Vorticity characteristics of the turbulent intermediate wake. *Expts. Fluids* **20**, 383–392.

Moin, P. 1990 Similarity of organized structures in turbulent shear flows. In *Near Wall Turbulence* (ed. S. J. Kline and N. H. Afgan), pp. 2–6. Hemisphere.

Moin, P. & Spalart, P. R. 1987 Contributions of numerical simulation data bases to the physics, modelling, and measurement of turbulence. *NASA TM* 100022, NASA-Ames.

Monin, A. S. & Yaglom, A. M. 1975 *Statistical Fluid Mechanics*, MIT Press.

Ong, L. & Wallace, J. M. 1995 Local isotropy of the vorticity field in a boundary layer at high Reynolds number. In *Advances in Turbulence V* (ed. R. Benzi), pp. 392–397. Kluwer.

Parantheon, P., Petit, C. & Lecordier, J. C. 1982 The effect of thermal prong-wire interaction on the response of a cold wire in gaseous flows (air, argon and helium). *J. Fluid Mech.* **124**, 457–473.

Perry, A. E., Lim, K. L. & Henbest, S. M. 1987 An experimental study of the turbulence structure in smooth- and rough-wall boundary layers. *J. Fluid Mech.* **177**, 437–466.

Piomelli, U., Balint, J-L. & Wallace, J. M. 1989 On the validity of Taylor's hypothesis for wall-bounded flows. *Phys. Fluids* A **1**, 609–611.

Pumir, A. & Shraiman, B. J. 1995 Persistent small scale anisotropy in homogeneous shear flows. *Phys. Rev. Lett.* **75**, 3114–3117.

Rajagopalan, S. & Antonia, R. A. 1993 RMS spanwise vorticity measurements in a turbulent boundary layer. *Exps. Fluids* **14**, 142–144.

Robinson, S. K. 1991*a* Coherent motions in turbulent boundary layer. *Ann. Rev. Fluid Mech.* **23**, 601–639.

Robinson, S. K. 1991*b* The kinematics of turbulent boundary structure. *Tech. Rep.* 103859. NASA-Langley.

SADDOUGHI, S. G. & VEERAVALLI, S. V. 1994 Local isotropy in turbulent boundary layers at high Reynolds number. *J. Fluid Mech.* **268**, 333–372.

SHAFI, H. S. & ANTONIA, R. A. 1995 Anisotropy of the Reynolds stresses in a turbulent boundary layer on a rough wall. *Exps. Fluids* **18**, 213–215.

SHAFI, H. S., ANTONIA, R. A. & KROGSTAD, P.-Å. 1995 Influence of surface roughness on the turbulence characteristics of a boundary layer. In *Proc. Tenth Symposium on Turbulent Shear Flows* (ed. J. C. Wyngaard, F. Durst, R. M. C. So & J. H. Whitelaw), pp. 5.13–5.18.

SHAFI, H. S., ZHU, Y. & ANTONIA, R. A. 1997 Statistics of $\partial u/\partial y$ in a turbulent wake. *Fluid Dyn. Res.* **19**, 169–183.

SHE, Z. S., JACKSON, E. & ORSZAG, S. A. 1988 Scale-dependent intermittency and coherence in turbulence. *J. Sci. Comput.* **3**, 407–434.

SPALART, P. R. 1988 Direct simulation of a turbulent boundary layer up to $R_\theta = 1410$. *J. Fluid Mech.* **187**, 61–98.

SREENIVASAN, K. R. 1991 On local isotropy of passive scalars in turbulent shear flows. *Proc. R. Soc. Lond.* A **434**, 165–182.

SREENIVASAN, K. R. 1996 On the universality of the Kolmogorov constant. *Phys. Fluids* **7**, 2778–2784.

SREENIVASAN, K. R. & ANTONAI, R. A. 1997 The phenomenology of small-scale turbulence. *Ann. Rev. Fluid Mech.* **29**, 435–472.

SUZUKI, Y. & KASAGI, N. 1990 Evaluation of hot-wire measurements in turbulent wall shear flows using a direct numerical simulation data base. In *Engineering Turbulence Modelling and Experiments* (ed. W. Rodi and E. N. Ganic), pp. 361–370. Elsevier.

TAVOULARIS, S. & CORRSIN, S. 1981 Experiments in nearly homogeneous turbulent shear flow with a uniform mean temperature gradient. Part 2. The fine structure. *J. Fluid Mech.* **104**, 349–367.

UBEROI, M. S. 1957 Equipartition of energy and local isotropy in turbulent flows. *J. Appl. Phys.* **28**, 1165–1170.

VAN ATTA, C. W. 1991 Local isotropy of the smallest scales of turbulent scalar and velocity fields. *Proc. R. Soc. Lond.* A **434**, 139–147.

VEROLLET, E. 1972 Etude d'une couche limite turbulente avec aspiration et chauffage à la paroi. PhD Thesis, Université d'Aix-Marseille II.

VINCENT, A. & MENEGUZZI, M. 1991 The spatial structure and statistical properties of homogeneous turbulence. *J. Fluid Mech.* **225**, 1–20.

VUKOSLAVCEVIC, P. & WALLACE, J. M. 1981 Influence of velocity gradients on measurements of velocity and streamwise vorticity with hot-wire X-array probes. *Rev. Sci. Instrum.* **52**, 869–879.

WALLACE, J. M. & FOSS, J. F. 1995 The measurement of vorticity in turbulent flows. *Ann. Rev. Fluid Mech.* **27**, 469–514.

WESTBURY, P. S. 1996 The effect of Reynolds number and wall roughness on bursts in turbulent boundary layers. PhD Thesis, Imperial College of Science, Technology and Medicine.

WYGNANSKI, I. & FIEDLER, H. 1969 Some measurements in the self-preserving jet. *J. Fluid Mech.* **38**, 577–612.

WYNGAARD, J. C. 1969 Spatial resolution of the vorticity meter and other hot-wire arrays. *J. Sci. Instrum.* **2**, 983–987.

WYNGAARD, J. C. & TENNEKES, H. 1970 Measurement of small scale structure of turbulence at moderate Reynolds number. *Phys. Fluids* **13**, 1962–1969.

YAGLOM, A. M. 1981 Laws of small-scale turbulence in atmosphere and ocean (in commemoration of the 40th anniversary of the theory of locally isotropic turbulence). *Izv. Atmos. Oceanic. Phys.* **17**, 919–935.

ZHU, Y., ANTONIA, R. A. & KIM, J. 1993 Velocity and temperature derivative measurements in the near-wall region of a turbulent duct flow. In *Near-Wall Turbulent Flows* (ed. R. M. C. So, C. G. Speziale and B. E. Launder), pp. 549–561. Elsevier.